Single qubit dephasing in the many-body localization phase transition

Petri Liimatta
University of Oulu
Nano and Molecular Systems Research Unit
Theoretical Physics
2021

Abstract

We are interested in a model for quantum computer that consists of superconducting qubits, transmons. These transmons are known to experience decoherence which causes unwanted dynamics in their quantum state. In this thesis, one form of decoherence experienced by the transmon, dephasing, is studied. The goal of this research is to differentiate the thermalization phase from the many-body localization phase in a transmon chain by studying dephasing of a single transmon. This phase transition is measured by simulating an array of transmons using the Bose–Hubbard model and calculating the dephasing rate R_2 that a single transmon experiences. The many-body localization is shown to have significantly reduced dephasing rates compared to the rates observed at the thermalization phase in three different cases with varying ratio between the interaction strength and the hopping rate $U/J = 2$, 3.5 and 5. From these results we see that the phase transition is seen when the disorder strength is in the range of $W/J = 10 - 15$ on all three cases. An interesting future outlook could be to study the deeper features of the phase transition by examining the the effect of spin-echo pulses on the transmon dephasing.

Contents

1 Introduction

The advancement of technology has improved the circuitry of classical computers nearly to the point where the world of quantum mechanics starts to interfere with their design. To further improve the computing capacity of a computer, recent attention has shifted onto the research of quantum computing, a topic with a theoretical background under way for the last two decades.

A quantum computer [1] is a device which would operate much like a classical computer, but with the advantage of being able to process information utilizing the quantum mechanics. This method of computation has been theoretically proven to be more advantageous than its classical counterpart in many cases such as quantum simulation of molecules or factoring of large numbers. The research of quantum computers has advanced to the point where we can create a small ensemble of qubits - the equivalent of bits in a classical computer - and perform simple quantum algorithms on them.

One proposed realization for an ensemble of qubits would be the intuitive extension of circuitry to superconducting circuits [2]. These circuits operate at low temperatures, where the metal achieves the superconducting state. In this state, the electricity in the circuits does not experience voltage loss due to the resistance, making the application of quantum mechanics to the metal possible one quanta at a time. One such experimental setup consists of an array of superconducting circuits built for the purpose of quantum computing: transmons [3].

Currently the development of quantum computers utilizing the transmons is focused on reducing the effect of an unfortunate consequence of this approach: the decoherence. The transmon device is built to be subject to outside influences, causing it to experience decoherence [4]. A result of this decoherence is that the quantum state of a transmon evolves towards a statistical average, making it eventually lose any information it might have previously held. A recent experimental articles have shown the lifetime of a transmon to approach 100 μs [5].

Another way of looking at the decoherence is through a phase called thermalization. In a general case, thermalization means that a quantum system evolves to a state where every eigenstate of its Hamiltonian is equally likely to be measured. In the case of an ensemble of qubits the eigenstates of the system would be combinations of the states $|0\rangle$ and $|1\rangle$ resembling the state of the memory of a classical computer in bits. This means that the thermalization drives the ensemble of qubits towards the statistical average, scrambling the

memory completely.

Fortunately, there is another phase that counteracts the decoherence caused in the thermalization phase of the transmon. A certain phase transition can cause the system to enter in a phase in which the unwanted evolution of the state of the transmon is slowed down significantly. This phase is called the many-body localization [6–8], being a system-wide phenomenon similar to the Anderson localization [9]. An ensemble of interacting qubits achieves a phase transition from the thermalization to many-body localization depending on the disorder within the ensemble and the nature of its interactions.

The reason the many-body localization appears at high disorders is that the interactions are not likely to cause excitations between transmons with high energy difference, effectively reducing the effect of decoherence. Achieving the many-body localization in an array of transmons is therefore wanted in order to reduce the effect of decoherence. Recent experiments on an array of transmons have been able to realize this many-body localization phase [10–12].

In this thesis we study an array of transmons that is subject to one form of decoherence: dephasing. We particularly study a singular transmon in an array of transmons and its phase transition and especially the effect of dephasing onto it. The phases of the singular transmons are characterized by the rate at which the state of the transmon decays towards a thermalized state. This study is experimentally relevant, as we parameterize the simulation of an array of transmons with parameter ratios which are commonly used in experimental studies of transmons. These ratios create a scenario in which the array of transmons mimics the real-world experiments.

We begin the thesis by introducing the needed mathematical concepts in chapter 2. From there we move to chapter 3 in which we review the qubit and construct the transmon, as well as put the transmons into an array formation. In chapter 4 we introduce the topics of decoherence and dephasing in addition to the interactions between the transmons in the array. Chapter 5 introduces the phases of thermalization and many-body localization respectively. Lastly, in chapter 6 we introduce the simulation we use to study the phase transition to many-body localization and in chapter 7 we conclude the thesis by presenting the simulation results. In the end we look at some of the recent research relevant to the topics discussed in previous chapters.

2 Mathematical background

The state of a quantum mechanical system is usually expressed as a wavefunction $\psi(x)$ or as a state vector $|\psi\rangle$ [13, 14]. In this chapter the notation of the state vectors is expanded to include more complicated states. These so-called density operators are introduced which leads to the matrix representation of the state.

The matrix representation is then used along with the tensor products to construct operators that operate to multiple states at once. This then leads to operators that are used to deal with systems consisting of multiple quantum objects. The purpose of these operators is to model parts of our system, for example multiple harmonic oscillators or interactions between quantum objects.

Later the theory of probability is worked on to construct tools for analyzing non-deterministic behaviour of a variable. This leads to random walk and its characteristics. The autocorrelation function is introduced and used to calculate one of the main interests of the random walk: the spectral density function.

2.1 Review of state vectors

Let us review what we know about the state vectors. The state vector $|\psi\rangle$ belongs to an n-dimensional complex Hilbert space $\mathcal{H}$. The Hilbert space has a base $|1\rangle, |2\rangle, ..., |n\rangle$ in which the state vector is expressed along with complex coefficients $c_1, c_2, ..., c_n \in \mathbb{C}$, giving the representation

$$|\psi\rangle = \sum_{i=1}^{n} c_i |i\rangle \in \mathcal{H}. \tag{1}$$

This expression is in general valid for more than just the physical systems, so the state vector needs something else in order to be a valid representation of a quantum system. Like the wavefunctions, the state vectors are limited with the normalization condition

$$\langle\psi|\psi\rangle = 1 \iff |c_1|^2 + |c_2|^2 + ... + |c_n|^2 = 1, \tag{2}$$

where $\langle\psi| = |\psi\rangle^\dagger$.

2.1.1 Density operator

The density operator is a matrix that is constructed with vectors. This procedure is made by taking the *outer product* of the vector with itself. In the following, let us denote a matrix constructed by a vector $|v\rangle$ as $\hat{M}_v$. This matrix is defined as a outer product of its vector

$$\hat{M}_v = |v\rangle \langle v| , \tag{3}$$

giving an $n \times n$-dimensional square matrix. The elements of this matrix are products of the coordinates of the vector as

$$(\hat{M}_v)_{ij} = c_i c_j^*. \tag{4}$$

The diagonal elements of the density operator are real, as we are taking the norm of the complex coefficients there. The same can not in general be said for the off-diagonal elements, since the phases of c_i and c_j^* don't necessarily cancel each other.

Operating on a vector $|u\rangle$ with the matrix $\hat{M}_v$ produces a projection onto the direction of the vector $|v\rangle$.

$$\hat{M}_v |u\rangle = |v\rangle \langle v|u\rangle = \cos\theta e^{i\varphi} |v\rangle , \tag{5}$$

where the angle θ is the angle between vectors $|v\rangle$ and $|u\rangle$ and φ is a complex phase factor. This makes the density operator a projection operator.

In quantum mechanics, we require that the operators we use are Hermitian. This condition means that the Hermitian transpose of a matrix must be equal to the matrix itself. Because we are dealing with state vectors, fortunately the density operator is by definition Hermitian

$$\hat{M}_v^\dagger = (|v\rangle \langle v|)^\dagger = \langle v|^\dagger |v\rangle^\dagger = |v\rangle \langle v| = \hat{M}_v.$$

Another requirement, the normalization condition, needs also to be filled as the density operator consists of the state vectors. This condition reduces to

calculation of the *trace* of the matrix. Due to the nature of the state vectors, the trace of the density operator is equal to the norm of the state vector

$$\mathrm{Tr}(\hat{M}_v) = \mathrm{Tr}(|v\rangle \langle v|) = \sum_{i=1}^{n} \langle i|v\rangle \langle v|i\rangle = \sum_{i=1}^{n} c_i c_i^* = \langle v\rangle = 1.$$

As the matrix constructed by a vector fulfills our requirements for a physical representation of a quantum system, we can conclude that the density operator can be used to express the state of a quantum mechanical system. With this, we construct the *density operator* [14] as

$$\hat{\rho} = \sum_i p_i |i\rangle \langle i| . \tag{6}$$

We determine the constants p_i to be the probability for the system to be at a state $|i\rangle$. Note that this definition does not necessarily lead to a density operator which is a diagonal matrix. However, the density operator is diagonal in the basis $|i\rangle$.

2.1.2 Tensor product

When we are dealing with a system of multiple quantum objects, we need to distinguish the state of the whole system from the individual states. As we have well-established state-vector notation for the states of single quantum objects, we could think about expressing the state of the whole system by using these individual states. For this purpose we introduce the tensor product. The tensor product is used to combine two vectors (generally two tensors of the same order) into a new vector that spans the space of both of its components. The tensor product $\otimes$ is defined for two vectors $|v\rangle \in \mathcal{H}_v, |u\rangle \in \mathcal{H}_u$ as

$$|v, u\rangle \equiv |v\rangle \otimes |u\rangle \in \mathcal{H}_v \otimes \mathcal{H}_u. \tag{7}$$

The vector $|v, u\rangle$ has coordinates $|v\rangle$ in the space $\mathcal{H}_v$ and $|u\rangle$ in the space $\mathcal{H}_u$. The basis vectors of *tensor product space* $\mathcal{H}^2$ are the vectors $|i, j\rangle$ with $i = 1, .., n$ and $j = 1, .., n$. For example, the vector $|1, 2, 3\rangle$ is in the space $\mathcal{H}^3$ with individual vectors being $|1\rangle, |2\rangle$ and $|3\rangle$ in their own spaces.

Taking tensor product of two general vectors $|v\rangle = \sum_{i=1}^{n} c_i |i\rangle$ and $|u\rangle = \sum_{j=1}^{n} u_j |j\rangle$ results in the vector

$$|v,u\rangle = |v\rangle \otimes |u\rangle = \sum_{i=1}^{n}\sum_{j=1}^{n} c_i u_j |i,j\rangle . \tag{8}$$

By combining the state vectors of individual states of the quantum system, we obtain a state that expresses the combined state of the whole quantum system. Looking at the definition of the tensor product, the individual state vectors can be also reclaimed by taking an inner product with respect to the other spaces.

For example, in order to extract the vector $|v\rangle$ from the vector $|v,u\rangle$, one has to take the inner product with $\langle u|$ (notice that the inner product is operating to the latter term)

$$\langle u| \cdot |v,u\rangle = \sum_{i,j,k=1}^{n} u_i^* c_j u_k \langle i| \cdot |j,k\rangle = \sum_{i,j,k=1}^{n} u_i^* c_j u_k \delta_{i,k} |j\rangle \tag{9}$$

$$= \sum_{i=1}^{n} |u_i|^2 \sum_{j=1}^{n} c_j |j\rangle = \langle u\rangle |v\rangle = |v\rangle .$$

In this example we see that operating with the state $|u\rangle$ produced its norm as it operated to the product space. The last line is a result of working with normalized state vectors, as we are dealing with quantum mechanics. Another concern is where the inner product is operated. Calculating the previous example by taking the inner product with the first term gives $\langle u| \cdot |v,u\rangle = \langle u|v\rangle |u\rangle$.

As with vectors, the matrices can also be combined using the tensor product. This is particularly important, because the operators in quantum mechanics are expressed with matrices. With the state of the whole quantum system, we could apply operators to the system as a whole instead of having to worry about the individual state vectors. Here we are not interested in how the combination works, just the results. The resulting matrix operates to the product space. For example, consider a matrix $\hat{O} = \hat{\sigma}_z \otimes \hat{I}$. This matrix operates to the vector $|v,u\rangle$ as

$$\hat{O} |v,u\rangle = (\hat{\sigma}_z \otimes \hat{I})(|v\rangle \otimes |u\rangle) = (\hat{\sigma}_z |v\rangle) \otimes (\hat{I} |u\rangle) = (\hat{\sigma}_z |v\rangle) \otimes |u\rangle . \tag{10}$$

Looking at the result we see that the first operator of the matrix operated to the first vector with $\hat{\sigma}_z$ and the second operated to the second vector with $\hat{I}$. We see that even if the matrix was operating to the product space, the calculation reduced to applying the operators to the individual states.

With this tensor multiplication we can construct matrices that operate only on certain vectors in the tensor product space simply by applying the operator $\hat{I}$, as it does nothing. Later we use this to construct the Hamiltonian of the system we are interested.

2.2 Probability

The measurement of a physical quantity often results in a value that is not exactly the correct, expected result. This error in measurement can be caused by many factors, for example due to the inaccuracy in the measuring device or the small environmental changes to the measured system. In this thesis we are studying dephasing, which causes a particular change to our system of interest.

The errors in physical quantities can be expressed as a random variable, giving the deviation from the expected value. In this chapter we express these random variables with the letter η. The study of the randomness caused by these random variables is expressed in terms of the theory of probability [15]. Here we go through a particular aspect of the theory of probability, namely the random walk.

2.2.1 Random walk

The most common example of a *random walk* is a process in which a variable either increases or decreases by one at random on each step of the process. Mathematically speaking, if we take a random variable η_i (that is either 1 or -1) on the i:th step of the process, the random walk l_N at the N:th step of the process is

$$l_N = \sum_{i=1}^{N} \eta_i. \tag{11}$$

The random walk can be characterized by the distribution of the random variable η. Since the process is linear, the expectation value of the random walk is the sum of the expectation values of η. This would mean that $\langle l_N \rangle = N \langle \eta \rangle$.

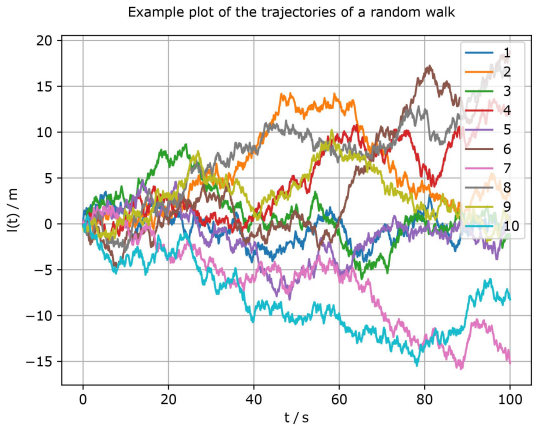

Figure 1: Ten example realizations of trajectories of random walks where the displacement of the random walk l is plotted as a function of time t using Eq. (12) where η is taken from an uniform distribution in the interval [-0.5,0.5].

For example, if we were to take the displacement η from a continuous uniform distribution between 0 and 1, we would get that $\langle \eta \rangle = 1/2$. With this, we could calculate that the expectation value of the random walk is $\langle l_N \rangle = N/2$. What this example tells us is that the expectation value of the random walk l_N can be derived from the expectation value of the random variable η. This feature is crucial in determining the underlying randomness in a given random walk.

A random walk can also be continuous, taking in random variables $\eta(t)$ at each time t. This case would be more physical, as a discrete random walk would mean that the randomness varies in discrete steps. A continuous random walk $l(t)$ would then be expressed as an integral

$$l(t) = \int_0^t \eta(t')dt'. \tag{12}$$

An example of a continuous random walk is given in Fig. 1, where a number of realizations of the random walk is plotted. In this example η is taken from an uniform distribution from -0.5 to 0.5. This would mean that the expectation value of the random walk would be $\langle l(t) \rangle = \int_0^t \langle \eta(t') \rangle \, dt' = 0$. Note that even if the expectation value is zero, it does not mean that a realization of the random walk itself would necessarily be at zero after time t.

An additional complication to the random walk can also be noted: the random variable $\eta(t)$ can, in principle, depend on the time t. The time-dependence can

be due to something physical, for example the electromagnetic field, or other continuous or even discrete variables. A random variable that is not dependent on time is called a *static random variable*, meaning that the randomness is not time-dependent.

A random walk itself can also depend on time t, independently of the random variable η. If we can observe the time-dependence of the random walk, we can say that it has a *memory*. This memory means that we can tell the difference between $l(t_1)$ and $l(t_2)$ for a given t_1 and t_2. For example, in our random walk in Fig. 1 we can see that the random walk has some memory, because $l(t_1)$ and $l(t_2)$ are relatively close when t_1 is close to t_2. However, at long time differences the value of $l(t)$ starts to be hard to predict, making it lose memory of a distant past.

The memory of a random walk can be predicted from its graph, but it would be more beneficial to express this condition also mathematically. The dependence of a random value from another random value is called *correlation*. A specific correlation, *autocorrelation*, tells how much the variable η depends of itself at two different times t and $t + \tau$.

The autocorrelation function at times t and τ is defined by the expectation value of the product $l(t)l(t + \tau)$, or as an equation

$$R(t, \tau) = \langle l(t)l(t + \tau)\rangle_l \,, \tag{13}$$

where $l(t)$ is a realization of the random walk at time t and the average is taken over all realizations. If the variable η is a static random variable, the time dependence is only due to the value of τ. This simplifies the autocorrelation function by averaging over time t

$$R(\tau) = \langle R(t, \tau)\rangle_t = \langle\langle l(t)l(t + \tau)\rangle_l\rangle_t \,. \tag{14}$$

In the case of the continuous random walk, the autocorrelation function in the case of a static random variable is

$$R(\tau) = \langle l(t)l(t + \tau)\rangle_t = \frac{1}{T}\int_0^T \langle l(t)l(t + \tau)\rangle_l \, dt, \tag{15}$$

where T is the total time taken by the random walk.

Note that the autocorrelation is a function of time and it tells how correlated the studied random walk is at a specific time τ. High amount of correlation over time tells us that the random walk has memory.

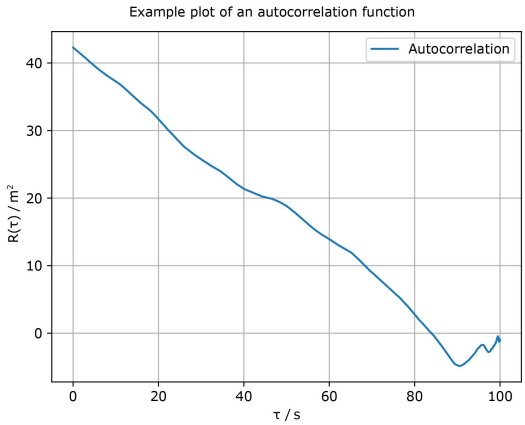

Figure 2: An example plot of an autocorrelation function, where the autocorrelation R is plotted against time τ using Eq. (15). The random walks used in this calculation are plotted in Fig. 1.

Calculating the autocorrelation for the random walk realizations in Fig. 1, we obtain the autocorrelation function shown in Fig. 2. We see that the autocorrelation decreases over time, meaning that the correlation is smaller in the end.

2.2.2 Noise

A particular application of random walk is noise. Coincidentally, we later express our errors in the system with this noise. In otherwise steady process noise is general interference which causes the process to deviate from its path. Usually noise is associated with sound but it can be found elsewhere, like in electrical signals or as unevenness of a road.

The noise is modeled as a random walk with the equilibrium being the intended value of the process. Here we assume that the random variable η is taken from a distribution with zero average. To begin analyzing the noise, we calculate its autocorrelation function. However, plotting the autocorrelation gives little info, as it tells how correlated the noise is at each point in time. To see how much different timescales contribute to the correlation, we use the Fourier transform.

The Fourier transform of the autocorrelation gives us a spectrum where the proportional appearance frequencies of each time scale is plotted. This spectrum is given a special name, the *spectral density function* $S(\omega)$, and it is calculated as

$$S(\omega) = \mathcal{F}(R(t))(\omega) = \int e^{i\omega t} R(t) dt. \tag{16}$$

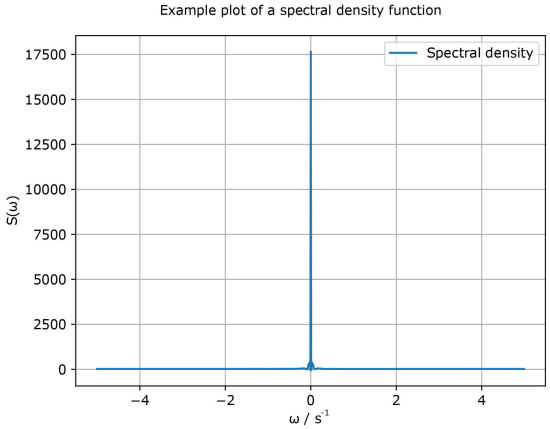

Figure 3: An example plot of the spectral density function of Eq. (16), where the spectral density S is plotted against frequency ω. The autocorrelation R is taken from Fig. 2.

Continuing analyzing the random walk from Fig. 1, we note that in our example the distribution of the random variable η does indeed have an average of zero. This makes it a candidate for a noise, so we take the Fourier transform of the autocorrelation function from Fig. 2 to get the spectral density shown in Fig. 3. Note that in general the Fourier transform is complex function and here we are interested only in its real part.

From Fig. 3 we see that the spectral density is highly concentrated on the zero-frequency area. This means that only the smallest possible time scales play a role in the memory of the random walk in our example. In another words, this random walk has short memory, remembering only what its few previous positions were.

The noises are categorized by their spectral densities. The most common noise is the white noise, which has a constant spectral density. The white noise has no memory and hence no correlation, so the autocorrelation of a white noise is a delta function $R_W(t) = \sigma^2 \delta(\tau)$ (σ^2 is the variance of the noise).

Fourier transform shows that the spectral density of a white noise is a constant $S(\omega) = \sigma^2$. In the example that we have been using during this chapter, the noise is not a white noise.

The noise in which we are interested in this work is the pink noise (or $1/f$-noise) [16, 17]. This noise is defined with the intensity of the spectral density to be inversely proportional to its frequency $S(\omega) = 1/f^\alpha, \alpha \in [0, 2]$, close to 1. The $1/f$-noise is common in many physical systems, notably those which interact with electric field.

3 Qubit

In this section we introduce the qubit and start heading towards the main topic of this thesis. The real world qubit design is introduced through a *transmon* device [3, 14], which is the state-of-the-art qubit realization within superconducting quantum technologies. These transmons are then put to an array to illustrate, for example, the memory of a quantum computer.

The qubit is a two-level system. This means that it has only the ground state $|0\rangle$ and one excited state $|1\rangle$, with state vectors of the form $|\psi\rangle = \alpha\,|0\rangle + \beta\,|1\rangle$ for some coefficients $\alpha, \beta \in \mathbb{C}$ with the normalization condition $|\alpha|^2 + |\beta|^2 = 1$. The squares $|\alpha|^2$ and $|\beta|^2$ are interpreted as the probability for the qubit being in state $|0\rangle$ or $|1\rangle$.

The Hamiltonian of a qubit is $\hat{H} = \hbar\omega\hat{\sigma}_z$, and from this we can calculate the time evolution of the qubit according to the Schrödinger equation. In the basis $\{|0\rangle, |1\rangle\}$ the Schrödinger equation gives

$$i\hbar\frac{d\,|\psi\rangle}{dt} = \hat{H}\,|\psi\rangle = \hbar\omega\hat{\sigma}_z(\alpha\,|0\rangle + \beta\,|1\rangle). \tag{17}$$

In the Scrödinger picture, the state vectors are time-dependent and the operators do not change over time. Since the basis is independent of time, for the solution to exist the coefficients α and β need to be time-dependent. From this follows that

$$\begin{aligned} i\hbar\frac{d\,|\psi\rangle}{dt} &= i\hbar(\alpha'(t)\,|0\rangle + \beta'(t)\,|1\rangle) \\ &= \hbar\omega(\alpha(t)\,|0\rangle - \beta(t)\,|1\rangle). \end{aligned} \tag{18}$$

Since the basis is orthogonal, by taking the inner product on both sides with $\langle 0|$ and $\langle 1|$, the problem separates to a group of equations

$$\begin{cases} i\hbar\alpha'(t) = \hbar\omega\alpha(t) \\ i\hbar\beta'(t) = -\hbar\omega\beta(t) \end{cases}, \tag{19}$$

which are easy to solve. The solution gives

$$\begin{cases} \alpha(t) = \alpha_0 e^{-i\omega t} \\ \beta(t) = \beta_0 e^{i\omega t} \end{cases}, \tag{20}$$

where the normalization condition applies at all times t and α_0 and β_0 are the initial values for the coefficients. This means that for all $t \in \mathbb{R}$, $|\alpha(t)|^2 + |\beta(t)|^2 = |\alpha_0|^2 + |\beta_0|^2 = 1$. From this solution we see that the qubit stays at the same (super)position as it was at the start. We also see that the states of the qubit oscillate in the complex plane with frequency ω.

Solving the eigenstates of the Hamiltonian gives the solutions $E_- = -\hbar\omega$ and $E_+ = \hbar\omega$. From this we can conclude that the ground state energy of the qubit is $-\hbar\omega$ and the energy of the excited state is $\hbar\omega$. The energy difference of these states is $2\hbar\omega$ and, if we shift the energies so that the ground state energy is at zero, we get the energy of the excited state to be the energy difference between the two states.

From another point of view, a harmonic oscillator has a similar feature: since all of its states are equally apart, by fitting the energy difference of the states of the qubit as the energy difference of the states of the harmonic oscillator, we can model the qubit with a harmonic oscillator. If we only consider the lowest two states, the harmonic oscillator acts like a qubit. This kind of harmonic oscillator has the Hamiltonian of a normal harmonic oscillator $\hat{H} = \hbar\omega\hat{n}$, but with allowed basis states being only $|0\rangle$ and $|1\rangle$.

Consider that we were to construct a real harmonic oscillator and use it to model a qubit, then it would not be prevented to escape into higher excitations. This is due to the harmonic energies: the state $|1\rangle$, when driven to by energy $\hbar\omega$, could get excited to state $|2\rangle$ in addition to getting lowered to state $|0\rangle$. In the qubit model this phenomenon is not allowed. We can however reduce the chances of this happening in certain kinds of quantum circuits. The transmon, as we derive it next, is a device that would exhibit the desired behaviour.

3.1 Cooper pair box

To construct a transmon device, we start with a superconducting junction, the Josephson junction [14]. This junction is composed of two superconducting materials that are separated by a thin layer of insulating material. This way the Josephson junction does not classically allow single electrons to pass through it.

However, there is a scenario in which a coupled pair of electrons can tunnel through it. This pair is called a Cooper pair. Cooper pairs appear in the

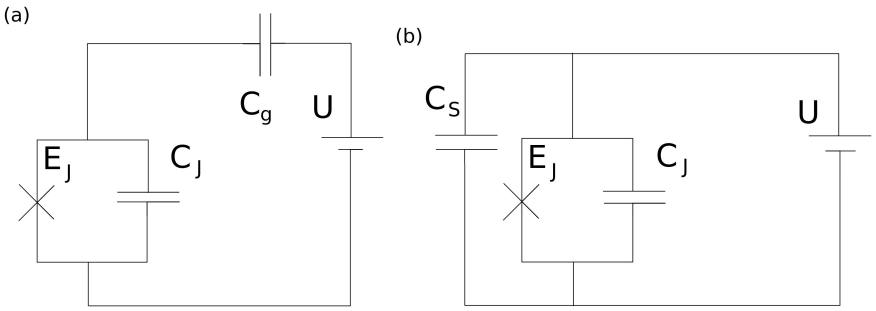

Figure 4: (a) Schematic of a Cooper pair box with tunneling energy (Josephson energy) E_J, capacitance C_J and gate capacitance C_g. (b) Schematic of a transmon device with Josephson energy E_J, capacitance C_J and shunt capacitance C_S. The gate charge is left out.

superconducting materials where the electrons of opposite spin and momentum pair up. Since Cooper pair is composed of two electrons, it holds a charge of $2e$ and has integer spin, which causes it to behave like a boson.

Putting a voltage through the Josephson junction creates a bias for the charge. This way the Cooper pairs are more likely to tunnel through one direction than the other. Note that classically a Josephson junction is no different from a regular capacitor.

By introducing an additional capacitor after the Josephson junction, a place forms into the circuit where classically charge can not change. This place is between the Josephson junction and the new capacitor and it is often called an "island" or a "box". Because the Josephson junction is a quantum mechanical circuit element, the charge of the island can change as a result of a tunneling event. To model the Josephson junction in a circuit design, we separate the tunneling effect to its own components and add parallel to that a capacitor that holds the capacitive features of the Josephson junction, as the Josephson junction acts classically like a capacitor. Overall, the circuit we are working with now is described in Fig. 4(a).

The other capacitor is called the gate capacitor as it acts as a gate to the island with the Josephson junction. This circuit is then called the *Cooper pair box*. Through quantum circuit analysis, the Hamiltonian of this system can be calculated. The Hamiltonian of the Cooper pair box depends on the energy required for a Cooper pair to tunnel through the Josephson junction E_J, the gate capacitance C_g and the junction capacitance C_J. With these parameters,

the Hamiltonian is

$$\hat{H} = \frac{(Q_0 - \hat{Q})^2}{2(C_J + C_g)} - E_J \cos \frac{2\pi\hat{\Phi}}{\Phi_0}, \tag{21}$$

with $\Phi_0 = h/2e$ being the flux quantum where h is the Planck constant and e is the elementary charge. The operators $\hat{Q}$ and $\hat{\Phi}$ are the charge and flux operators in analogy to the momentum and position operators $\hat{p}$ and $\hat{x}$. Lastly, the variable Q_0 is the bias charge on the island.

A more practical way to present the Cooper pair box is to introduce its Hamiltonian in the charge basis $|n\rangle$, where the n represents the quanta of charge on the island. In this basis, the Hamiltonian is

$$\hat{H} = \sum_n \left[4E_C \left(n + \frac{Q_0}{2e} \right)^2 |n\rangle \langle n| - \frac{E_J}{2} (|n+1\rangle \langle n| + |n-1\rangle \langle n|) \right]. \tag{22}$$

We see that the capacitive energy $E_C = \frac{1}{2}e^2(C_J + C_g)$ is related to the energy of each state and the Josephson energy acts as an energy threshold for the change of charge in the island.

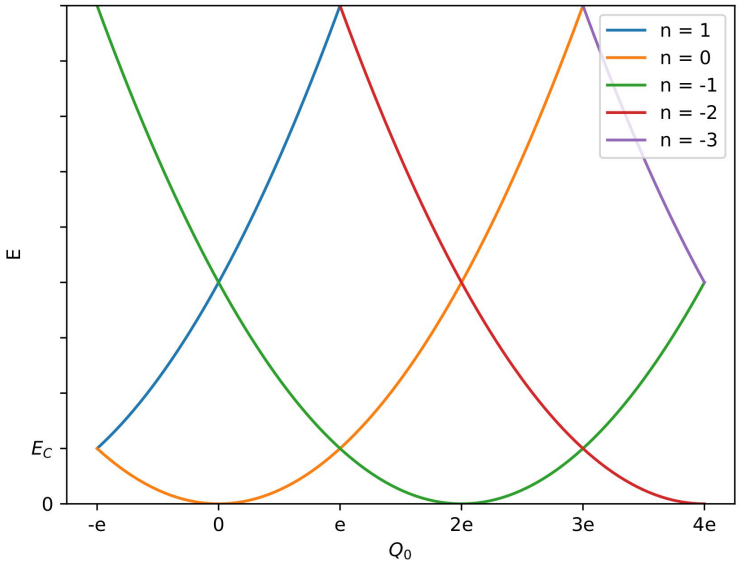

Figure 5: Energy of the states $|n\rangle$ in a Cooper pair box as a function of bias charge Q_0 where $E_J = 0$.

Solving the Hamiltonian of the Cooper pair box leads to a solution where the energy depends on the bias charge Q_0. The energy graph is shown in Fig. 5,

where we have drawn the energies of charge basis states $n = -3, .., 1$. Since the island takes electrons with charge $2e$, the energy minima are found where $Q_0 = 2en, n \in \mathbb{Z}$. This causes the energy graph to look like a set of parabolas, each having their minimum at some multiple of $2e$.

When the tunneling energy E_J is at zero, the parabolas cross each other particularly at odd multiples of e (Fig. 5). When the tunneling energy is increased, the crossing points of the parabolas separate and the graph forms multiple oscillating bands (Fig. 6). The way to use the Cooper pair box as a qubit would be to tune the island charge to be at odd multiple of e. This way the first two states are relatively close in energy and the next state would be far off.

3.2 Transmon

In practice the Cooper pair box interacts with the environment and as a result the bias charge Q_0 varies. This variation leads to a change in the energy difference between the states of the Cooper pair box. Since the operating energy would be approximately constant, the change in the qubit energy would affect its readability. To stabilize this situation we need to make the Cooper pair box less dependent on the charge. This way the changes in charge do not lead to changes in the energy differences.

The proposed way to decrease the charge dependency is introduced in Ref. [3]. The dynamics of the Cooper pair box are dependent on the ratio between the Josephson energy E_J and the charging energy E_C. The value of E_J/E_C needs to be optimized as the charge dispersion of the Cooper pair box decreases exponentially with respect to this ratio while the anharmonicity of the Cooper pair box is lost in according to a weak power law decay of this ratio.

The way to configure E_J/E_C is either to make changes to the Josephson energy or to the charging energy. The Josephson energy is difficult to change as the underlying Josephson junction itself needs to be remade. The easier process is to change the charging energy. As this energy is inversely proportional to the sum of the capacities of the Cooper pair box ($E_C = e^2/2C_{\text{tot}}$), it can be configured by adding an additional capacitor to the device. This additional capacitor is added parallel to the Josephson junction so that in Eq. (21) the denominator of the first term gets an additional capacitance C_S. The circuit we are now examining is shown in Fig. 4(b).

Examining the ratio E_J/E_C results in a lower limit of 20 according to Ref. [3]. In this limit the charge dependency in the lowest states is nearly gone and the

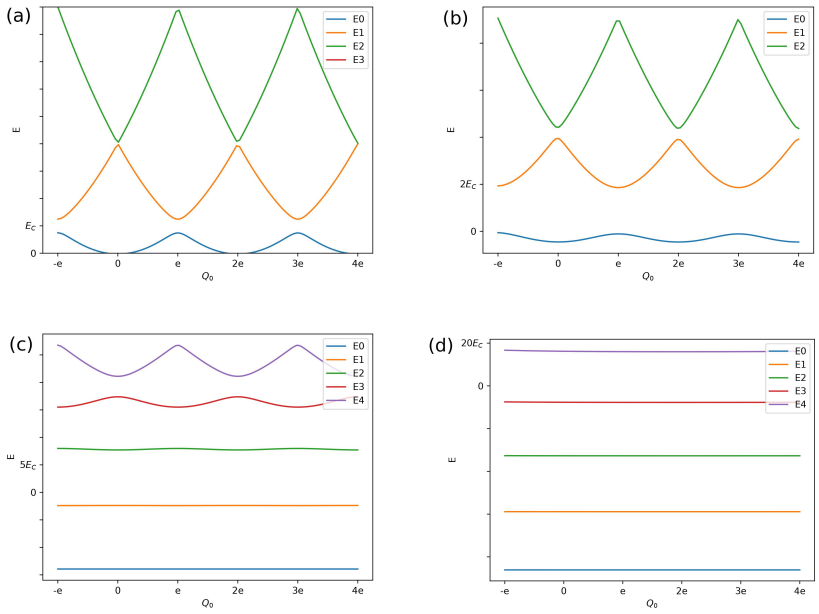

Figure 6: Energies of a transmon device as a function of bias charge Q_0 as the ratio E_J/E_C is (a) 0.5, (b) 2, (c) 20 and (d) 100.

charge fluctuation disrupts the Cooper pair box only slightly and any increase in E_J/E_C only reduces this further. On the other hand the upper limit of the ratio E_J/E_C is calculated to be $5 \cdot 10^4$ [3]. However this limit is far off, so it is usually practical to cut the favorable range to 100. With these conditions the device is called a *transmon* and the limit of E_J/E_C from 20 to 100 is called the *transmon limit*.

Although the transmon is independent of the bias charge Q_0, it is still a system of many states. To treat the transmon as a qubit we need to have a device that has only two states. The transmon does indeed act as a two-state system, but it may be unintuitive as how it manages to do that. To understand this phenomenon we need to look into the *anharmonicity* of the transmon. The transmon is not a harmonic system as its energies are not equally separated. The energies as a function of charge are horizontal lines that get closer to each other as the energy increases as seen in Fig. 6.

As we learned previously, the qubit has the energy difference of $\hbar\omega$. As the transmon is anharmonic, we can look the energy differences from another point of view: if we mark the energy difference of the ground state and the first excited state as $\hbar\omega$, the energy difference between the first and the second excited state

can be seen as $\hbar\omega - \epsilon$. The difference between these two differences is the energy ϵ, which is caused by the anharmonicity. If we were to operate on the transmon with precise energy $\hbar\omega$, it would cause a change between the ground state and the first excited state, but not with the second or higher excited states. This is caused by the quantum mechanics: a system can only receive certain quantum of energy. From this we can conclude that if we operate the transmon with precise energies, it acts as a two-level system.

In practice this phenomenon, anharmonicity, is modeled in the Hamiltonian of the system with the term $-\hbar\frac{U}{2}\hat{n}(\hat{n}-1)$. Calculating the energy contribution of this term gives out negative answer at higher energies but zero at the two lowest state. This way the anharmonicity does not affect the lower states of our system, which we are interested in. Putting this term together with the term for the harmonic oscillator, we get a model for the transmon as an anharmonic oscillator. The Hamiltonian of this system then is $\hat{H} = \hbar\omega\hat{n} - \hbar\frac{U}{2}\hat{n}(\hat{n}-1)$. The term U is called the *anharmonicity* of the transmon.

3.3 Many qubits

In quantum computers, the information is not stored only on single qubits but to an array of them. These arrays are then changed through quantum algorithms to obtain the wanted functionality. If we want to deal with multiple qubits at once, we must use state vectors that encapsulate the whole qubit array. These state vectors are made by utilizing the tensor products introduced in chapter 2.1.2.

If we have n qubits, their combined state vector is $|\psi\rangle = \otimes_{i=1}^{n} |\psi_i\rangle$, where the $|\psi_i\rangle$ is the state vector of the i:th qubit,

$$\begin{aligned} |\psi\rangle &= |\psi\rangle_1 \otimes |\psi\rangle_2 \otimes ... \otimes |\psi\rangle_n \\ &= (\alpha_1 |0\rangle + \beta_1 |1\rangle) \otimes ... \otimes (\alpha_n |0\rangle + \beta_n |1\rangle) \\ &= \alpha_1\alpha_2...\alpha_n |00...0\rangle + \beta_1\alpha_2...\alpha_n |10...0\rangle + ... + \beta_1\beta_2...\beta_n |11...1\rangle . \end{aligned} \tag{23}$$

The length of this state vector is 2^n because every qubit contributes its two states to the total sum. Given that the basis of every qubit is $\{|0\rangle, |1\rangle\}$, the total state vector can be expressed like on the last line of Eq. (23).

In this vector the basis states are $|\delta_1\delta_2...\delta_n\rangle$, with $\delta_i = 0$, or 1, so that each basis vector represents a specific configuration of n classical bits. These basis vectors are then multiplied with the products of the coefficients of the single qubits so that each qubit contributes either α_i or β_i depending on the δ_i. This way we get that the total state vector of this array of length n is in superposition

of states where the information is in a bit form. Note that the entangled states can not be expressed as a tensor product of individual states.

The state of a qubit array evolves in time according to the Schrödinger equation as do all quantum systems. The Hamiltonian of this qubit array $\hat{H}_{\text{tot}}$ is constructed by summing together the Hamiltonians of the single qubits $\hat{H}_{\text{tot}} = \Sigma_{i=1}^{n} \hat{H}_i$. As these single qubit Hamiltonians are 2×2 matrices, they operate only to the single qubits (noted in chapter 2.1.2). To create the matrices that operate on the whole tensor product space, we simply need to multiply the single qubit Hamiltonian so that it operates to the total state vector while only changing the intended qubit.

The expansion of single-qubit Hamiltonians are made as follows: we multiply n 2-dimensional identity matrices $\hat{I} = \left(\begin{smallmatrix} 1 & 0 \\ 0 & 1 \end{smallmatrix}\right)$ together with the tensor product but we change the i:th term in this product to be the Hamiltonian of the i:th qubit. Mathematically this goes like

$$\hat{H}_i' = \hat{I}_1 \otimes \hat{I}_2 \otimes ... \otimes \hat{H}_i \otimes ... \otimes \hat{I}_n. \tag{24}$$

This is the computational way to go from single-qubit Hamiltonian to the total Hamiltonian. Do keep in mind that in general the transmon is not a two-level system but has also higher states. To account for these, we would need to expand the Hamiltonians and the identity matrices to be $m \times m$ matrices. However, for simplicity the transmons can be approximated to be a two-level system.

In our model for the array of transmons, the total Hamiltonian can now be expressed as

$$\hat{H} = \hbar \sum_i \left(\omega_i \hat{n}_i - \frac{U}{2} \hat{n}_i (\hat{n}_i - 1) \right), \tag{25}$$

with $\hat{n}_i$ being the number operator operating to the i:th qubit. Note that we do not explicitly write the tensor products and the identity matrices. From this Hamiltonian we see that each transmon is oscillating at its own frequency ω_i and the energies of these transmons make them anharmonic oscillators. An interesting note is that these transmons are not interacting. In order for the quantum algorithms to work, the qubits need to interact and exchange information and energy, changing their state. Exactly how we implement this interaction is the topic of the next chapter.

4 Open quantum systems

The model for the array of transmons as anharmonic oscillators is not complete, as it does not include the interactions between different qubits. In this chapter

we dive into the interactions between quantum systems, mainly between the quantum system and its environment. These interactions are derived with the help of density operators, introduced in chapter 2.1.1.

First we take a look at how the density operators work from the perspective of the quantum physics. This way we expand the theory and get tools for analyzing the quantum systems, leading us to the von Neumann equation. With this, we look at the qubit that interacts with its environment. The resulting *interacting* (open) quantum system is then analyzed to understand the phenomena behind it, specifically the coherence from which we get one of the main topics of this thesis, the *dephasing*.

The familiar bra-ket notation can be expanded using the density operators (density matrices) introduced in the Eq. (6). In this operator form, the diagonal matrix elements correspond to the squares of the components of the state vectors. These are now the probabilities of the particle being in a specific state. On the contrary, the meaning of the off-diagonal elements is not so clear. We will see their significance later.

For a qubit $|\psi\rangle = \alpha\,|0\rangle + \beta\,|1\rangle$, the density matrix is

$$\hat{\rho} = |\psi\rangle\langle\psi| = (\alpha\,|0\rangle + \beta\,|1\rangle)(\alpha^*\langle 0| + \beta^*\langle 1|) \tag{26}$$
$$= |\alpha|^2\,|0\rangle\langle 0| + \alpha\beta^*\,|0\rangle\langle 1| + \alpha^*\beta\,|1\rangle\langle 0| + |\beta|^2\,|1\rangle\langle 1|$$
$$= \begin{pmatrix} |\alpha|^2 & \alpha\beta^* \\ \alpha^*\beta & |\beta|^2 \end{pmatrix},$$

in the basis $\{|0\rangle, |1\rangle\}$.

Operating to the density matrix differs little compared to the state vectors. In the case of density operators, the operator $\hat{O}$ operates on both sides, changing both ket and bra parts of the density matrix

$$\hat{O}\hat{\rho}\hat{O}^\dagger = \sum_i p_i \hat{O}\,|i\rangle\langle i|\,\hat{O}^\dagger = \sum_i p_i\,|i'\rangle\langle i'| = \hat{\rho}'. \tag{27}$$

The expectation values are a bit more complicated. For operator $\hat{O}$, the expectation value is calculated by taking the trace from the product of the operator and the density matrix

$$\langle\hat{O}\rangle = \mathrm{Tr}(\hat{O}\hat{\rho}), \tag{28}$$

which is unintuitive as the expectation value for a given operator in the state vector representation is calculated by $\langle\hat{O}\rangle = \langle\psi|\,\hat{O}\,|\psi\rangle$. The similarity between this and Eq. (28) however can be proven with straightforward calculation. One useful property of trace to note is that its contents can be rearranged as long as they are in the same permutation $\mathrm{Tr}(\hat{A}\hat{B}\hat{C}) = \mathrm{Tr}(\hat{C}\hat{A}\hat{B}) \neq \mathrm{Tr}(\hat{C}\hat{B}\hat{A})$.

4.1 Master equation

The time evolution of the density matrix is no more complicated than the Schrödinger equation itself. By applying this equation to the derivative of the density matrix, we get the time evolution in the form of

$$i\hbar\frac{d\hat{\rho}}{dt} = i\hbar\left(\frac{d\left|\psi\right\rangle}{dt}\left\langle\psi\right| + \left|\psi\right\rangle\frac{d\left\langle\psi\right|}{dt}\right) \tag{29}$$

$$= i\hbar\left(-i/\hbar\hat{H}\left|\psi\right\rangle\left\langle\psi\right| + i/\hbar\left|\psi\right\rangle\left\langle\psi\right|\hat{H}\right)$$

$$= \hat{H}\hat{\rho} - \hat{\rho}\hat{H} = [\hat{H}, \hat{\rho}]$$

which is known as the *von Neumann equation*.

However, both the Schrödinger equation and the von Neumann equation assume that the system is not interacting with an outside environment. Therefore whatever the system is, it has unitary time evolution. This evolution does not account for the interaction between the system and its environment. More interesting and more realistic approach would be to include these interactions. To simplify the calculations it is useful to reduce the degrees of freedom of the environment which leads to the master equation.

We study this system with a model in which the studied system interacts with its environment (thermal bath or reservoir) that is assumed to be large. The interaction is expressed with the operator $\hat{C}$ and the strength of the interaction is indicated with a constant γ. We say that the interactions are dissipative when $\gamma > 0$, meaning that the system loses energy to the bath. Also we require that the time evolution of the system recovers its unitary evolution if $\gamma \to 0$.

In our model, we additionally require that the interaction between the system and the bath is weak compared to the internal dynamics of the system. The time evolution at zero temperature, under the rotating wave approximation and Born and Markov approximations, reduces to

$$\frac{d\hat{\rho}}{dt} = -\frac{i}{\hbar}[\hat{H}, \hat{\rho}] + \frac{\gamma}{2}(2\hat{C}\hat{\rho}\hat{C}^\dagger - \hat{C}^\dagger\hat{C}\hat{\rho} - \hat{\rho}\hat{C}^\dagger\hat{C}). \tag{30}$$

This equation is known as the *master equation* with the specific form begin the *Lindblad form* [14, 18]. The solutions of the master equation (30) are accurate when the approximations hold, meaning systems where high-frequency terms of the Hamiltonian can be neglected, the environment is not affected by the interactions with the system and the evolution of the system does not depend on its previous states.

In the case a qubit, the interaction with the environment can be described with the lowering operator $\hat{a}$. In an interaction picture, the master equation (30) reduces to

$$\frac{d\hat{\rho}}{dt} = \frac{\gamma}{2}(2\hat{a}\hat{\rho}\hat{a}^\dagger - \hat{a}^\dagger\hat{a}\hat{\rho} - \hat{\rho}\hat{a}^\dagger\hat{a}). \tag{31}$$

Solving the master equation (31) gives a solution in which the qubit loses energy to the environment because the occupation of the excited state decays. On the other hand, the ground state occupation grows as the excited state decays. The differential equations of these states can be interpreted as the system emitting a quantum of energy to the bath and in some circumstances absorbing a quantum of energy from the bath. The off-diagonal elements of the density matrix of the qubit are exposed to the so-called decoherence and decay to zero. Additionally they have a complex phase factor that depends on the frequency of the qubit ω.

4.2 Decoherence

As said before, the density matrix can be a mix of many different states. We can differentiate these *mixed states* from the states that are composed of only one state vector (*pure states*) by looking at the expectation value of the density matrix $\langle\hat{\rho}\rangle = \mathrm{Tr}(\hat{\rho}^2)$. For pure states, this expectation value is 1, but for the mixed states it is less than 1.

For example, consider two qubits $\hat{\rho}_1 = (|0\rangle + |1\rangle)(\langle 0| + \langle 1|)/2$ and $\hat{\rho}_2 = (|0\rangle\langle 0| + |1\rangle\langle 1|)/2$. We see that the $\hat{\rho}_1$ is composed of only one state vector, $(|0\rangle + |1\rangle)/\sqrt{2}$, but $\hat{\rho}_2$ is a sum of two states, $|0\rangle$ and $|1\rangle$. The density matrices can also be calculated in the matrix form, giving $\hat{\rho}_1 = \frac{1}{2}\left(\begin{smallmatrix}1 & 1\\ 1 & 1\end{smallmatrix}\right)$ and $\hat{\rho}_2 = \frac{1}{2}\left(\begin{smallmatrix}1 & 0\\ 0 & 1\end{smallmatrix}\right)$.

Calculating purity for the density matrix $\hat{\rho}_1$, $\mathrm{Tr}(\hat{\rho}_1^2)$, so that

$$\mathrm{Tr}\Big[\frac{1}{4}\begin{pmatrix}1 & 1\\ 1 & 1\end{pmatrix}\begin{pmatrix}1 & 1\\ 1 & 1\end{pmatrix}\Big] = \frac{1}{4}\mathrm{Tr}\Big[2\begin{pmatrix}1 & 1\\ 1 & 1\end{pmatrix}\Big] \tag{32}$$

$$= \frac{1}{2}\mathrm{Tr}\Big[\begin{pmatrix}1 & 1\\ 1 & 1\end{pmatrix}\Big] = \frac{1}{2}(1+1) = 1,$$

so the state $\hat{\rho}_1 = (|0\rangle + |1\rangle)(\langle 0| + \langle 1|)/2$ is indeed a pure state. On the other hand $\hat{\rho}_2$ gives $\mathrm{Tr}(\hat{\rho}_2^2) = 1/2$. Note that for both $\hat{\rho}_1$ and $\hat{\rho}_2$, the trace is 1.

Consider a sphere with radius 1 in the space $\{|0\rangle, |1\rangle\}$. In this sphere, the state $\hat{\rho}_1$ is on the surface of the sphere. This kind of superposition is called a coherent

superposition and $\hat{\rho}_1$ is said to be in a coherent superposition of multiple states. The state $\hat{\rho}_2$ on the other hand is an average of two states, $|0\rangle$ and $|1\rangle$, which leaves it on the inside of the sphere. This mixture of states is called a statistical mixture of states as we can think of the summing as averaging over the states. The state $\hat{\rho}_2$ is similarly called an incoherent statistical sum of multiple states.

The decoherence occurs when the off-diagonal elements of the pure states start to vanish. This happens in open quantum systems, where the master equation from Eq. (30) produces additional terms to the von Neumann equation. The result drives the pure state towards a mixed state. In our example, if we would put the state $\hat{\rho}_1$ into an open quantum system, it would over time go to the state $\hat{\rho}_2$.

4.3 Dephasing

One specific form of decoherence, the dephasing [3], is studied in this thesis. To understand the dephasing, we first look at the environmental noise that interacts with an open quantum system. In certain cases, the noise introduces a complex phase $e^{i\theta}$ to the state vector.

For example, take a state vector $|\psi\rangle = (|0\rangle + |1\rangle)/\sqrt{2}$. The complex phase factor could then change the state into $|\psi'\rangle = (|0\rangle + e^{i\theta}|1\rangle)/\sqrt{2}$. However, this change would not affect the diagonal elements of the density matrix so the effect would only be visible on the off-diagonal terms. The density matrix would then look like $\hat{\rho} = \frac{1}{2}\begin{pmatrix} 1 & e^{i\theta} \\ e^{-i\theta} & 1 \end{pmatrix}$.

Over time this phase factor drives the system to a different, mixed state. From a statistical point of view, since we do not know the phase θ, averaging over the phases results in loss of coherence. This kind of decoherence is then called dephasing.

Simply detaching the system from the environment is not enough as we would also lose the ability to read the state of the system. Another point of interest is that the other qubits interacting with a specific qubit can be considered as its environment.

4.4 Pulses

One way to counteract the decoherence is to apply electromagnetic pulses to the system. These pulses would change the system in a way that ends up cancelling

out the unknown phase, thus enhancing the coherence. A great deal of research has been conducted [19–23] and it has been found that these pulses do help in keeping the decoherence out of the system.

This phenomenon is explained in the simplest case to be caused by the reversal of the time evolution. A π-pulse along the x-axis in the middle of the time evolution flips the qubit state, making the Hamiltonian affect the qubit in a way resembling the reversal of the time evolution. This pulse is called a *spin-echo* sequence, originating from the theory of NMR [24].

The spin-echo is the simplest pulse sequence, but more complicated sequences have been developed in order to keep the decoherence low. A strong contender for this kind of sequence is a Carr–Purcell–Meiboom–Gill (CPMG) sequence, consisting of multiple equidistant π-pulses along either x or y-axis. The CPMG sequence is another one of the simplest NMR sequences, and it has been shown to perform well against decoherence [22, 23].

Yet another pulse sequence that has been studied is UDD, developed by Uhrig [20, 21]. This sequence employs dynamical decoupling (DD) [23] and it is specifically developed to counteract the effects of the decoherence. The UDD is a sequence of π-pulses along either x or y-axis, where the times between the pulses are not equal. The timings τ_i of the pulses are determined by

$$\tau_i = \tau \sin^2\left(\frac{\pi i}{2n+2}\right), \tag{33}$$

where the τ is the total time of the pulse sequence and the n is the total number of the pulses ($\tau_{n+1} = \tau$).

There is a connection between the spin echo, CPMG and UDD sequences: for $n = 1$ pulses the UDD is exactly the spin echo sequence, and for $n = 2$ the CPMG and UDD are equal. For a larger amount of pulses, the UDD is not divided into special pulse sequences. One curiosity is that the most important difference between the CPMG and UDD is the way their effect depends on the noise in the system. Previously we have discussed about the $1/f$ noise that is known to affect our system of interest. This noise is strongest at low frequencies, making the UDD sequence a top contender as it filters the low-frequency noise the best [22]. However, there is a case for the CPMG pulse sequence as well. If the noise in the system experiences a certain kind of cutoff, UDD filters it better than the CPMG [22, 23]. But, in the case where this cutoff is absent or it is not reached, the CPMG sequence performs better than UDD.

4.5 Coupled qubits

With all of these tools, we can continue developing the model for the system of interacting qubits. We left off at Eq. (25), where each transmon evolved over time independently through the Hamiltonian $\hat{H}_i = \hbar\omega_i\hat{n}_i - \hbar U/2\hat{n}_i(\hat{n}_i - 1)$. To include the interactions, we need to think what kind of interaction occurs between these transmons. Since the islands of the transmons have no physical contact with each other, we can expect that they do not transmit particles between each other. This leaves us with the exchange of energy.

The energy exchange between particles A and B can be seen as the following: A gets energy from somewhere at the same time as B loses the same amount of energy. We do not specify that the exchange happens between particles A and B, but, considering the energy can not be lost, we have an exchange of energy between these two specific particles. Then we ask, how much is this amount of energy? Quantum mechanics makes this question easy as the energy is quantitized.

Let us consider a harmonic oscillator, where the energy quanta is $\hbar\omega$. If we were to take a unit of energy out of this system, it would be done with the lowering operator $\hat{a}$. As we know, the lowering operator drops the energy of the harmonic oscillator by one unit in the "ladder". On the other hand, putting $\hbar\omega$ amount of energy to the harmonic oscillator can be achieved with the raising operator $\hat{a}^\dagger$, which is also the hermitian conjugate of the lowering operator.

Now, if we would have two harmonic oscillators A and B with the same energy intervals $\hbar\omega$, their interaction would be following: A gets $\hbar\omega$ by getting operated to its state with the raising operator and B loses $\hbar\omega$ with the lowering operator. Using two different states for both A and B makes the process hard to follow, so we switch to the state space of the total system: the tensor product space. Now we have a space, where the state vector is $|A, B\rangle = |A\rangle \otimes |B\rangle$. In this space, the raising and lowering operators are expressed as $\hat{a}^\dagger \otimes \hat{I}$ and $\hat{a} \otimes \hat{I}$ when operating to the A and $\hat{I} \otimes \hat{a}^\dagger$ and $\hat{I} \otimes \hat{a}$ when operating to B.

We said before that the energy exchange can be thought to occur instantly. This means that we operate to the A with raising/lowering operator as we operate with lowering/raising operator to the B. The operators responsible for these interactions are then $\hat{a} \otimes \hat{a}^\dagger$ and $\hat{a}^\dagger \otimes \hat{a}$, where the first operator takes a quanta out of A and puts it into B and the second operator does the opposite. If we look closely at the definitions, we can see that the operators specify the flow of energy only one way.

Generally speaking, we do not know which way the energy is flowing or if it is

flowing at all. However, we can think of these interactions as small perturbations to the system, as mentioned previously. This lets us approximate the energy exchange to happen to both ways equally. Because of this approximation, we can introduce the coupling term as $\hat{a}_A\hat{a}_B^\dagger + \hat{a}_A^\dagger\hat{a}_B$, where the tensor product is hidden. The indexes A and B note which harmonic oscillator the operator is acting on. This coupling operator puts our system into a superposition of two states, where the energy is shifted either from A to B or from B to A.

Lastly, how does the likelihood of an energy exchange to happen show up in this consideration? Similarly to the coupling strength γ in master equation (30), the rate at which interaction happens can be taken as a strength of the interaction as if it happened constantly over time. Therefore, let us mark the parameter that defines the coupling strength as J. This changes the coupling operator to $J(\hat{a}_A\hat{a}_B^\dagger + \hat{a}_A^\dagger\hat{a}_B)$.

For the transmons, the above arguments apply. In the case of two transmons, the coupling term would look like $J(\hat{a}_1\hat{a}_2^\dagger + \hat{a}_1^\dagger\hat{a}_2)$. For n transmons the term operating to the first transmon would look like $J(\hat{a}_1\hat{a}_2^\dagger + \hat{a}_1\hat{a}_3^\dagger + ... + \hat{a}_1\hat{a}_n^\dagger + \hat{a}_1^\dagger\hat{a}_2 + \hat{a}_1^\dagger\hat{a}_3 + ... + \hat{a}_1^\dagger\hat{a}_n)$. Making a simple argument that the interactions are short-distant causes the further terms ($\hat{a}_1\hat{a}_k^\dagger$ and $\hat{a}_1^\dagger\hat{a}_k$, $k = 3, 4, ..., n$) to vanish quickly. This simplifies our interaction so that we can write the general coupling term as $J(\hat{a}_i\hat{a}_{i+1}^\dagger + \hat{a}_i^\dagger\hat{a}_{i+1})$ for the i:th qubit, excluding the last one, since we do not have the $(n+1)$:th qubit. Note that the coupling between qubits $|i\rangle$ and $|i-1\rangle$ is included in the $(i-1)$:th term, so that we do not double count the interactions.

Now that we have the coupling between the qubits figured out we can introduce the total Hamiltonian of the array of interacting qubits. The Hamiltonian for n transmons is

$$\hat{H} = \hbar\sum_{i=1}^{n}\omega_i\hat{n}_i - \hbar\frac{U}{2}\sum_{i=1}^{n}\hat{n}_i(\hat{n}_i - 1) + \hbar J\sum_{i=1}^{n-1}(\hat{a}_i\hat{a}_{i+1}^\dagger + \hat{a}_i^\dagger\hat{a}_{i+1}), \tag{34}$$

where the parameter U is the anharmonicity of the system and J is the coupling (hopping) strength. The equation Eq. (34) is known as the *Bose–Hubbard model*. We will be using this model in our computation to model the array of transmons. But before we get to the modeling the array, we need to go over the last theoretical part so that we get a good understanding of what we are after.

5 Thermalization

The Bose–Hubbard model (Eq. 34) is known to exhibit many phases depending on the values of anharmonicity U and the interaction strength J, and the system itself. Two of these phases, described with thermalization and localization, are studied [6–9, 19, 25] with the interest being towards the localization. In this chapter we study this phenomenon, starting from a statistical point of view. The goal is to understand what do we mean by thermalization and localization and how they each affect the dynamics in a transmon array. As a starting point, let us remind ourselves of the statistical physics.

In statistical physics, the starting point of understanding the dynamics of many-body systems is introduced with the postulate of *a priori* probabilities. This postulate says that an isolated system in equilibrium is equally likely to be found in any of its accessible microstates. By microstates we mean a certain configuration of the particles that constitute the system. Mathematically, the postulate of a priori probabilities means that if we have a system with N possible microstates, then every one of those states $i = 1, ..., N$ appears with the same probability $p_i = 1/N$.

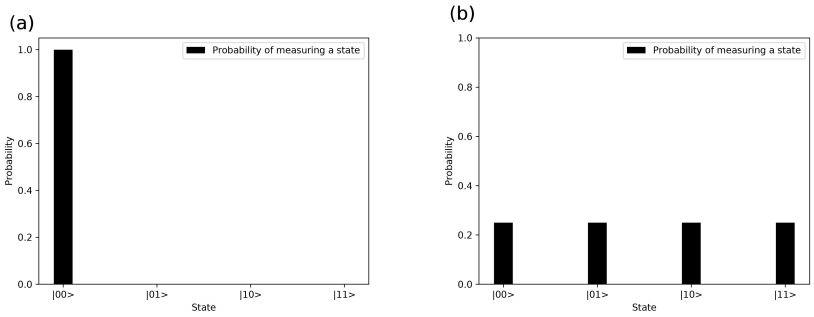

Figure 7: An illustrative example of a closed quantum system of two qubits exposed to thermalization. In panel (a), the system is in state $|00\rangle$. In panel (b), the system is in thermal state.

In quantum physics, a microstate means a state in which each particle is in certain superposition, that may be unknown. The postulate of a priori probabilities in quantum physics means that every possible state appears with equal probability. A quantum system that is in this kind of state is said to be *thermalized*. An example of thermalized system could be a closed quantum system of two qubits with all of its possible eigenstates being $|00\rangle, |01\rangle, |10\rangle$ and $|11\rangle$. As the system is closed, it does not interact with the environment. Inside of this system, the thermalization happens, making all of the states equally likely to be measured.

This means that the probability of measuring any of the states of this system, $|00\rangle, |01\rangle, |10\rangle$ or $|11\rangle$, is $1/4$ or 25%.

Another related, but not the same, topic is the *eigenstate thermalization hypothesis* [6]. This hypothesis states that the eigenstates of a generic many-body quantum system thermalize. This means that if we have a quantum system with N eigenstates and it obeys the eigenstate thermalization hypothesis, all of the eigenstates of the system have the probability $1/N$ of being measured. Continuing our example, if we would prepare a closed system of two qubits in state $|00\rangle$, then unitary many-body dynamics would lead to the thermalized state according to the eigenstate thermalization hypothesis. This is illustrated in Fig. 7, where in Fig. 7(a), the system is prepared to the previously mentioned state. After some time, in Fig. 7(b), the state can be seen to be the thermal state as all of the states of the system are equally likely to be measured.

Considering our point of interest, the array of transmons that act as qubits, the thermalization would eventually lead to a loss of information. For an array of N transmons, the thermalization drives the system towards a state where the probability of measuring any local configuration is $1/N$. This being the case, the thermalization should be eliminated from the array in order to preserve information over a long time. However, the thermalization is a statistical phenomenon and as such it is difficult to get rid of.

However, the eigenstate thermalization hypothesis is just a hypothesis and as such it does not necessarily hold. This means that there could exist a quantum system whose eigenstates do not thermalize. This kind of system would then preserve its information over a long time and could be used, for example, as a memory in a quantum computer.

To differentiate between this new, exotic system and the systems that we have discussed, we note that statistically this change in phenomenology is viewed as a phase transition. The phase transition, as described in statistical physics, is an abrupt change in the dynamics or other properties of the system. With the phemonena regarding the thermalization, this definition is good because as it catches the essence of what we are studying. Hence we say that the systems that thermalize are in a *thermalized phase*. In the next section we will see what is this new, non-thermalized system.

5.1 Localization

Consider a system that does not thermalize. This system then has at least one state that does not approach the themalization condition. For example, if we

were to make our example of two qubits into this kind of system, then it could have a state, for example state $|00\rangle$, that does not thermalize. Since this state does not thermalize, the chance of it being measured could be artificially tuned to, for example, 0. What follows from this is interesting: if we were to now separate the two qubits and measure the first qubit to be at the state $|0\rangle$, we would know that the second qubit is at the state $|1\rangle$, since the only possible state of the system that has the first qubit at the state $|0\rangle$ is the state $|01\rangle$.

However, this kind of system is not our point of interest. The notion of tampering with one arbitrary state in a quantum system is not practical. We need to take into account that we are dealing with a physical system. A more interesting application of this non-thermalizing phase would be to restrict a single particle in the system, so that its individual state would not change even if the rest of the system would thermalize.

This kind of phenomenon is called *localization* and it was first observed by P. W. Anderson [9]. The localization described by Anderson focuses on single entity (occupation of a site in a lattice) of a quantum system. Practically, this means that each site is defined by the occupation of electrons or other particles in the site. In his article, Anderson mentions silicon atoms as an example for these sites. The energies of the sites are needed to be random variable distributed over some probability distribution which can be characterized by a single variable, width W. This produces a stochastic aspect to this problem. Lastly, the sites can interact with each other but not with the environment, making the system a closed quantum system.

The singular site then experiences the potential of its neighborhood and is expected to thermalize. However the occupation of the site retains some of its original amplitude over time. Anderson points out this phenomenon coming from the fact that if the energy of the sites is random, the interactions fail to cause an exchange due to unfavorable gaps in energy. If no exchange of energy happens, the amplitude of the state is conserved which leads to the occupation of the site preserving its state over time. The localization in which only a single site is preserved in this way is called the *Anderson localization*.

This means that we can produce a closed quantum system in which there exists a singular site whose state does not decay over time. In our example of two qubits the Anderson localization would therefore allow us to preserve the state of a single qubit. Let us Anderson localize the first qubit to state $|0\rangle$. This would mean that the first qubit does not experience thermalization, while the second qubit thermalizes over time. If we were to put the system in state $|00\rangle$, over time the system would gravitate towards a state where the probability of measuring states $|00\rangle$ and $|01\rangle$ would be equal. This would be because the first

qubit is localized and thus does not change its state, whereas the second qubit thermalizes, making it equally likely to be measured on both states $|0\rangle$ and $|1\rangle$.

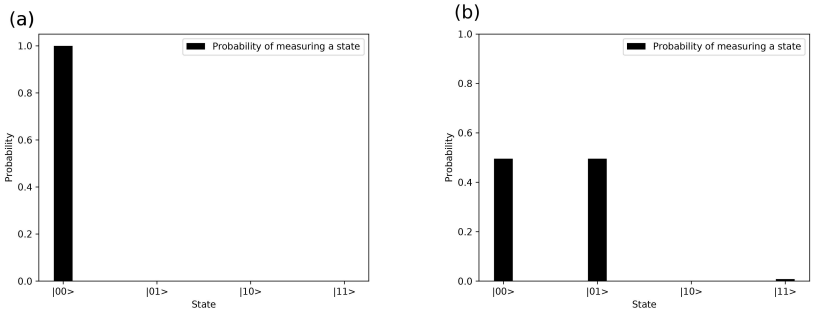

Figure 8: An illustrative example of a closed quantum system of two qubits exposed to localization. In panel (a), the system is in state $|00\rangle$. In panel (b), the system has localized the first qubit, but not the second one.

Another illustrated example of this is in Fig. 8, where in Fig. 8(a) the system is initially in the state $|00\rangle$. After some time, we see the effect of the localization on the first qubit in Fig. 8(b). Since the second qubit does not localize, it thermalizes, leaving the system in a superposition of states $|00\rangle$ and $|01\rangle$. In a real-world scenario the interactions from outside affect the localization slightly: there might exist a small probability that we measure an unexpected result (see Fig. 8(b), the probability of state $|11\rangle$). The small fluctuating chance can be usually neglected as it does not usually grow large enough to be of importance.

Now, how do we see the effects of the Anderson localization on the array of transmons that we are interested in? Turns out that the Anderson localization is not what we are after. As previously discussed, the array of transmons has interactions between excitations, causing transmission of energy regardless of the Anderson localization phase. What we need to do is study the system as a whole to determine whether it experiences a similar localization phenomenon as the Anderson localization. This kind of localization is discussed in the next section, where we look at expanding the knowledge gained from the Anderson localization to construct the *many-body localization*.

5.2 Many-body localization

The many-body localization is a phase of an interacting quantum system [6,8,25] in which, in addition to the Anderson localization, the different sites are allowed to interact with each other. This interaction allows the whole system to experience

localization. The many-body localized system can be modeled by using the Bose–Hubbard model (Eq. 34), where the energy of each site is random, as in the Anderson localization. These energies are taken from an uniform distribution, characterized by width W. Together with the interaction strength U the Bose–Hubbard model can be tuned to model the many-body localized system.

The many-body localization is a high-energy phase [6], meaning that there is essentially no difference between bosonic and fermionic quantum systems when this phase is studied. This allows us to treat the many-body localization with either bosonic or fermionic system. Taking the bosonic system and limiting the Hilbert space to two dimensions, we get to use qubits as our sites when studying this phase. The array of transmons that we are interested in is this way a proper system where the many-body localization can happen.

The way the many-body localization avoids thermalization is linked to the interactions [6] in addition to the Anderson localization phenomenon. If no couplings are present (at $J = 0$), the system is just a chain of non-coupled anharmonic oscillators. This means that the state of the whole system is in product state $|\psi_0\rangle \otimes |\psi_1\rangle \otimes |\psi_2\rangle \otimes ...$ and the individual sites can be viewed as independent systems, each of which is Anderson localized.

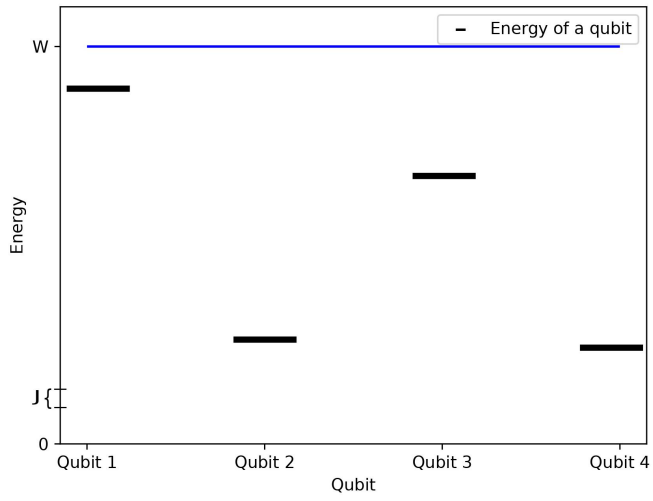

Figure 9: Example of a difference between the parameters W and J in a many-body localized array of four qubits. The energy of the qubits is taken from an uniform distribution from 0 to W and the ratio W/J is 20.

For $J \neq 0$ the regime where $J \ll W$, the perturbations caused by the couplings

are small compared to the energy splitting caused by the randomness in energy. As a result, no thermalization occurs because the random energy gap between sites is large for the couplings to be effective. This is illustrated in Fig. 9, where we can see the differences in energy being larger than the coupling strength J. Note that this argument is similar to the one Anderson used [9], when describing the single-site localization scheme.

From this we can conclude [6], that for sufficiently large ratio W/J, the transport of spin and energy is absent, causing no thermalization to happen. This argument is perturbative (small J) and is backed by numerical evidence [6], which is not limited by the coupling strength J.

A significant difference to the Anderson localization is that the local phase does not last but starts to delocalize logarithmically [6]. This means that the thermalization can be reached eventually, but the process slows down significantly over time. The delocalization is due to the couplings within the system and causes decoherence. The decoherence has been studied [26], and it is found to be caused by a noise on the system, specifically the $1/f$-noise noted in the chapter 2.2.2.

The phase transition between the thermal phase and the many-body localized phase is marked to be an eigenstate phase transition [6, 8, 25], which means that the eigenstates are being observed to change their behaviour when transitioning from one phase to the other. To study this phase transition, one needs to use a disorder ensemble of only one eigenstate, because the transition is dynamic. For a phase transition to be dynamic means that it is not observable by traditional statistical mechanical ensembles, as it averages quantities, making the phenomena undetectable.

The modeling of the many-body localization has been done using the the Bose–Hubbard model (Eq. 34) with appropriate parameters. The realizations has been both computational [7, 8] and experimental [25]. The ratio W/J has been taken to be in the regime $W/J \gg 1$, varying between implementations.

Lastly, there exists a so-called "mobility edge" on the many-body localization [6]. This edge means a threshold in energy of systems where not all of the eigenstates are localized. Above the mobility edge, the states of the system are in thermalized phase, obeying the eigenstate thermalization hypothesis. This means that the localized states are all below a certain energy. It is also possible to construct a system whose states are thermalized only below a certain energy, creating an inverted mobility edge [6].

6 Simulating the array of transmons

In this section, we introduce the simulation of the array of transmons. The programming language chosen is Python 3.8, with the usage of the Python library QuTiP [27, 28], version 4.5.2.

The computational simulation involves the Bose–Hubbard model (Eq. 34) with the option to vary the parameter ratio W/J. The ratio of anharmonicity to interaction strength U/J is taken to be 3.5 at the start of the simulations, corresponding to a typical experimental result on superconducting circuits. The Hamilton is divided by $\hbar J$ in order to achieve more manageable quantities. Taking all of these changes into account our Hamilton for the simulations will be

$$\frac{\hat{H}_{\text{comp}}}{\hbar J} = \sum_{i=1}^{L} \frac{\omega_i}{J} \hat{n}_i - \frac{U}{2J} \sum_{i=1}^{L} \hat{n}_i(\hat{n}_i - 1) + \sum_{i=1}^{L-1} (\hat{a}_i \hat{a}_{i+1}^{\dagger} + \hat{a}_i^{\dagger} \hat{a}_{i+1}), \tag{35}$$

for L transmons, where the energies ω_i are selected from the uniform distribution in $[-W, W]$. We select the energies of the transmons by taking uniform distributed random variable η and constructing the energy by

$$\omega_i = (1 - 2\eta)W, \tag{36}$$

where W is the maximum of the energy distribution, so that when $\eta \in [0, 1]$, $\omega_i \in [-W, W]$. This selection of energies ensures that the scaled energies ω_i/J are from the uniform distribution in $[-W/J, W/J]$.

The simulation of a quantum system on a classical computer is limited by the memory of the computer since we need to save the information of the whole system, specifically all of the complex numbers representing the quantum states. With density operators, the size of the system scales as $\mathcal{O}(k^{2L})$ for L k-state particles. Keeping track of thousands of frames, this starts to take a lot of memory. Therefore, we limit our system to a more manageable size of $6 - 9$ transmons. An additional limitation we assume to our simulation is that the number of allowed states is limited to a small number. This makes the transmons essentially act like qubits in the case where we only consider two states.

In order to start the simulation, we first initialize the system of transmons to the state

$$|\psi_0\rangle = |0\rangle \otimes |1\rangle \otimes |0\rangle \otimes |1\rangle \otimes ... = |0101...\rangle$$

We then construct the Hamiltonian for a chain of transmons between lengths 6 and 9 as we have previously explained in chapter 3.3.

6.1 Hamiltonian

The Hamiltonian is constructed by separating it into three parts. In the first part, we make a tensor product of identity matrices with the number operator $\hat{n}$ replacing one of them. Multiplied with the energy of the relevant transmon, this part is the $(\omega_i/J)\hat{n}_i$ in the first sum in Eq. (35), going over each transmon, these make up the first part of the total Hamiltonian. The second part of the Hamiltonian is constructed the same way as the first one, taking a tensor product of $6-9$ identity matrices and replacing one of them with the term $-(U/2J)\hat{n}_i(\hat{n}_i - 1)$.

The third and the last part of the Hamiltonian is constructed like the other two with the exception that the summing does not go over all of the transmons. The creation- and annihilation operators $\hat{a}^\dagger$ and $\hat{a}$ are taken as an interaction pair, taking place of two adjacent identity operators at a time. This makes the Hamiltonian one site too big, if it is not taken into account. From these, the total Hamiltonian is constructed by simply summing the three separate Hamiltonians together.

Lastly, the act of measurement is needed to be implemented in order to model the system as being measured. In this thesis we are interested in the evolution of single transmons, so we intend to measure the state of a single transmon. The model of this measurement is a $\hat{\sigma}_x$ operator operating onto the transmon of interest. To do this, we select one transmon to be measured. This transmon is taken to be at the middle of the transmon array. Technically, the measurement term is similar to the three Hamiltonian terms, being a tensor product of identity matrices with $\hat{\sigma}_x$ replacing one of them. The measurement probe acts to the array of transmons with Hamiltonian $\hat{H}_m = \hat{\sigma}_x^i \alpha \cos(\omega_i t)$, where the α is the strength of the probe and ω_i is the energy of the transmon being measured. We assume that the energy of the measured transmon is known beforehand. With this, we construct the Hamiltonian used in the simulations by combining the time-dependent measurement part with the time-independent Bose–Hubbard Hamiltonian.

6.2 The simulation

We are studying the single qubit dephasing in many-body localization. In order to get out the results of our measurement, we need to trace out the transmons we did not measure. The result is the state of the measured transmon. These states are averaged over realizations in order to inspect the average functioning of the system. This average is studied in this part, and in the next section we go over the results of this simulation.

The simulation parameters we chose were the following: the simulation time t was taken to be from 0 to $100J^{-1}$ with a time steps of $dt = 1/300J^{-1}$, the number of qubits was chosen to be 7, the ratio $U/J = 3.5$ as mentioned previously and the average was taken over 100 realizations. We extended the transmons to be three-state objects by increasing the number of allowed states to three, but focused only on the two lowest states and treated them as two-state objects. The measured qubit was the fourth transmon, having three other transmons on both sides of it.

If we were to simulate an array of transmons under the Bose–Hubbard model (Eq. 34) and view their dynamics, we would see that the expectation value of $\hat{\sigma}_z$, the population difference, of each two-state transmon would evolve over time like a damped cosine function. The cosine evolution is due to the Rabi oscillations and the exponential damping is due to the dephasing, caused by the third term in the Hamiltonian, the coupling term.

In a general case when taking into account the dephasing and dissipation of a driven qubit [29], we see that the population difference of the lowest two states should follow the curve

$$f(t) = [A\cos(\omega t) + B\sin(\omega t)]e^{-R_2 t} + C, \tag{37}$$

where ω is oscillation frequency, R_2 is the decay rate and A, B and C are parameters we are not interested in. In the simulations, we fit the data to the function $f(t)$ by calculating the value of $\langle\hat{\sigma}_z(t)\rangle = \hat{\rho}_{11}(t) - \hat{\rho}_{00}(t)$, where $\hat{\rho}(t)$ is the averaged density matrix of the studied transmon.

Out of the fitted parameters, we are interested in the decay rate R_2, which tells us how quickly the system is losing its coherence. The main point of our thesis is to study this parameter in order to determine the effect of the phase transition on its value.

The inverse of the decay rate is the *dephasing time* T_2, which measures how long a quantum state maintains its coherence. If we were to treat the dephasing as a noise to the transmon, we could derive a result which states that the inverse of

the dephasing time is proportional to the spectral density function of the noise at zero frequency $1/T_2 = 2S(0)$ [4].

The main aspect we take a look at is the many-body localization phase. This phase is differentiated from the thermalization phase in the simulations by the ratio W/J. In and out of the many-body localized phase, we expect the dephasing rate to differ due to the fact that the thermalization causes decoherence and quickly puts the system into the thermal equilibrium state.

7 Results and conclusions

In this chapter we conclude the study by extracting the relevant quantities out of the simulation results. We take a look into the dynamics of the transmon by evaluating the average state of the measured transmon that has evolved under different measurements. From these states, we calculate the population difference between the lowest two states and fit Eq. (37) to them in order to get out the dephasing rates R_2. We use these rates to differentiate between the thermalization and many-body localization.

7.1 Results

In the simulations, we first ran a test to determine if we could observe the phase transition from thermal phase to the many-body localized phase. This test was realized by varying the ratio W/J from 1 to 25 in steps of 1. Based on previous numerical observations [8] we expect that, at ratio $U/J = 3.5$, the thermal phase is present at $W/J = 1$ and the many-body localization appears at $W/J = 25$, in addition to the phase transition that is expected near $W/J = 8.5$. These phases would be realized by the values of R_2 being higher in the thermal phase than in the many-body localization.

Few example plots of the averaged population differences with the fitting functions Eq. (37) at ratio $U/J = 3.5$ are presented in Fig. 10, where the ratio $W/J = 5$ in Fig. 10(a), $W/J = 12$ in Fig. 10(b) and $W/J = 21$ in Fig. 10(c). In these three examples, the result for the dephasing rates were following: in Fig. 10(a), the results were $R_2 = (1.274 \pm 0.015)J$, in Fig. 10(b) $R_2 = (0.771 \pm 0.009)J$ and in Fig. 10(c) $R_2 = (0.043 \pm 0.001)J$.

In these examples and all of the other simulations, we took the error as the square root of the variance of the fitting. From these plots we can see that the

averaged population difference of the measured transmon oscillates in addition to the exponential decay caused by the dephasing. The exponential decay is stronger at lower ratios of W/J as expected.

At the thermal phase, we see the thermalizing effect being applied to the transmon we are observing in Fig. 10(a). This causes the population difference to decay to an equilibrium state. During the phase transition, the difference between the thermal phase and the many-body localization is not clear and we see this mixture in Fig. 10(b), where the exponential decay of the population difference is still quick due to the thermalization. The oscillation of the population difference becomes clearer as we increase the ratio W/J and in Fig. 10(c) we see this effect being only slightly damped by the exponential decay.

The dephasing rates of this numerical experiment are in the Fig. 11(a). From these we clearly see that the many-body localized phase has much lower value for the R_2, appearing after the phase transition that can be seen around $W/J = 10 - 15$. The differentiation between the two phases was successful, as the dephasing rates were an order of magnitude bigger in the thermalization phase. Additionally, the fact that the phase transition extends over a range of disorder ratios W/J could be a possible sign of a mobility edge [6, 12] mentioned before. Another possibility for this range is the initial configuration we chose for the system $|0101010\rangle$.

After we simulated the system with the ratio $U/J = 3.5$, we took a look at two additional systems, where we had chosen the ratios $U/J = 2$ and $U/J = 5$. From these simulations we looked at the phase transition to see if it would appear at different values of W/J. We expected the phase transition to appear near $W/J = 7.5$ at ratio $U/J = 2$ and near $W/J = 8.5$ at ratio $U/J = 5$ based on previous numerical observations [8]. The dephasing rates from these simulations are in Fig. 11(b) and Fig. 11(c).

The simulation results from the ratio $U/J = 2$ in Fig. 11(b) is not too different compared to the results of the ratio $U/J = 3.5$. The phase transition however can be seen from the $W/J = 11$ to $W/J = 16$, making it appear at slightly higher value of W/J than in the first case. On the other hand, the phase transition at $U/J = 5$ in Fig. 11(c) does not look to differ from the transition in $U/J = 3.5$. Both of these observations can also be accounted for the reasons we mentioned previously.

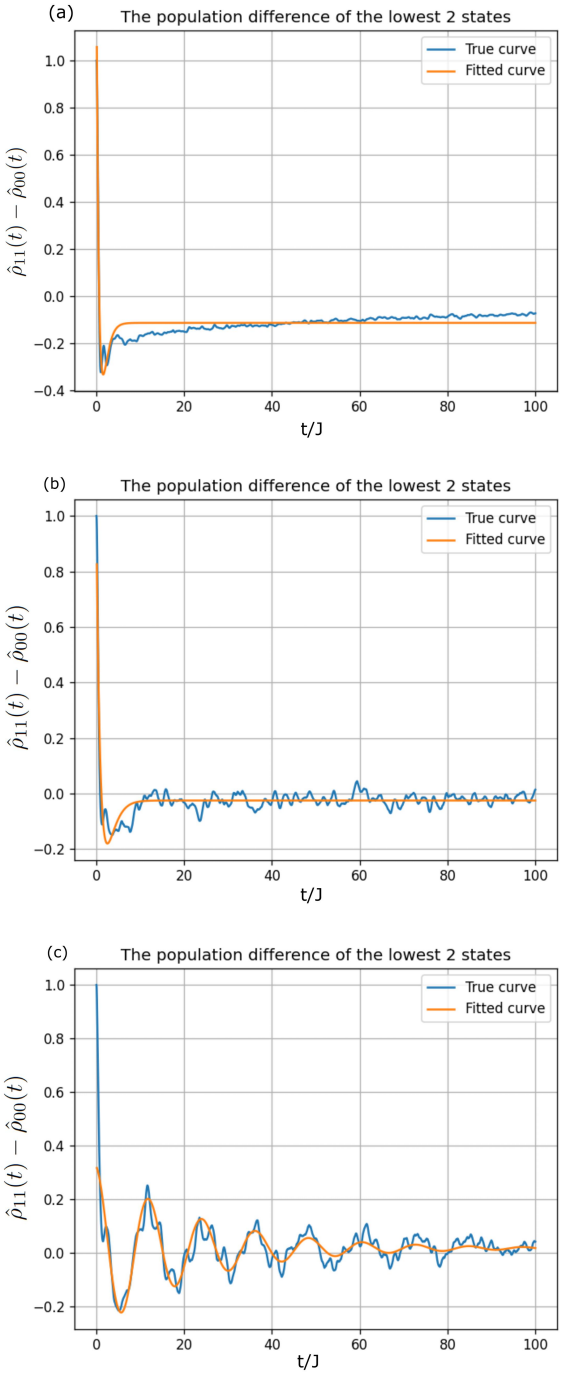

Figure 10: A few example plots of the averaged population differences as a function of time with the fitting functions Eq. (37) in which we have ratio W/J is (a) 5, (b) 12 and (c) 20.

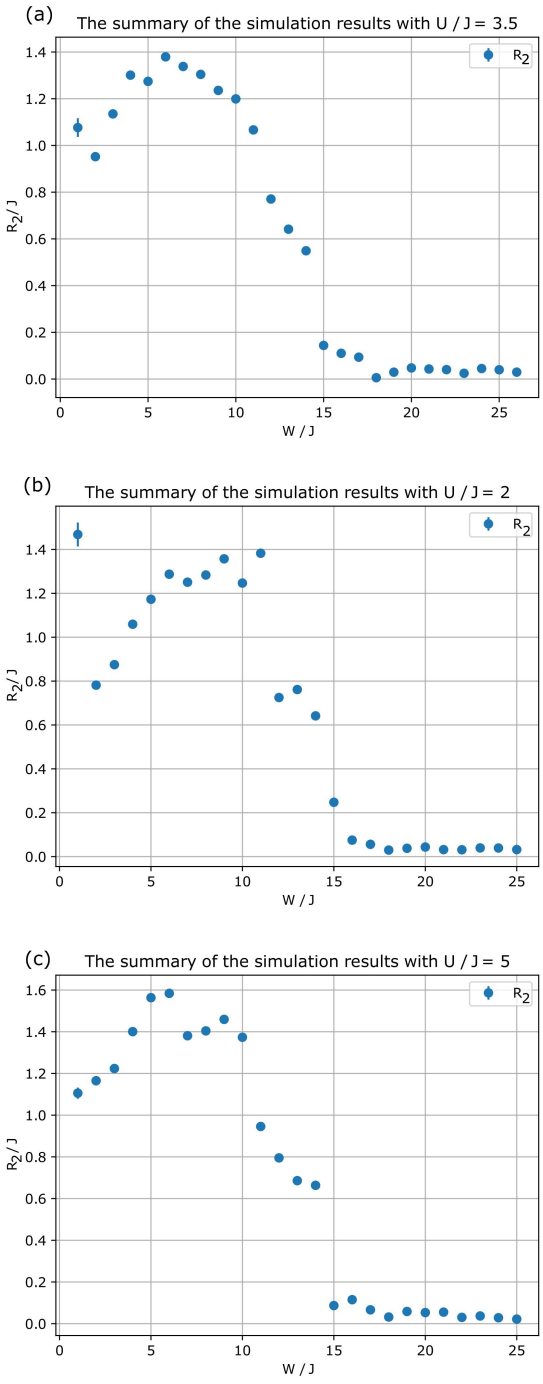

Figure 11: The dephasing rate R_2 as a function of the disorder strength W/J at different values of ratio U/J (a) 3.5, (b) 2 and (c) 5.

7.2 Conclusions

In this chapter we conclude the thesis by summarizing its contents as well as evaluating the success of the simulations and their results. The topic of this thesis was to study the phase transition between the thermalizing and many-body localized phase in an array of superconducting circuits, transmons. We began the theoretical work by broadening the mathematical background with the expansion of the bra-ket vector notation to include matrices, which we turned into the density operator representation of a quantum state, along with using the theory of probability to analyze an important realization of the random walk: noise.

Using the bra-ket notation, we started to talk about quantum mechanics and introduced the qubit. The motivation behind this chapter was to construct a real-world device that would work as close to a theoretical qubit as possible. Starting with a Cooper pair box, a simple superconducting qubit, we constructed a state-of-art quantum circuit: transmon. This anharmonic oscillator was proposed to be used as a qubit if we would only affect it with the precise energy equal to the difference between the ground state and the first excited state of the transmon.

The theoretically considered transmons were put into an array without accounting the couplings between the transmons. Motivated by the analogy of memory in the quantum computers, we wanted to make the transmon picture more realizable and interactable so the next topic we introduced was the coupling between a transmon and an environment and between transmons in an array. In quantum mechanics, the effects ot the interaction can be described with an open quantum system interacting with a general environment. For this purpose we used the density matrix representation and constructed the von Neumann equation of Eq. (29), which we further polished to get the master equation Eq. (30), specifically the Lindblad form of it.

Before making the transmons interactable we introduced an unfortunate consequence of the open quantum systems: decoherence. This encompassed all such interaction which would drive the quantum state of our transmons towards a statistic average, leading to the loss of any specific state. This would mean that, if implemented as the memory of a quantum computer, the transmons would eventually lose any stored information.

One form of decoherence that was of particular interest was the loss of average coherence: dephasing. The statistical result of averaging the quantum state resulted in decoherence even if singular realizations of transmons would turn out fine. While we did not implement it, one proposed way to counter the dephasing was introduced: pulses. Mimicking the theory of NMR, different pulse sequences

were introduced to reduce the effect of dephasing.

After pondering the decoherence we moved to the topic of coupling between the transmons. Since we can propose that the transmons are physically separate entities, the coupling between them was taken as the exchange of energy only. A few simple argument later we ended up with a model for this array of transmons which included both the anharmonicity and the interactions. This model is known as the Bose–Hubbard model, Eq. (34), and after introducing it we moved on to inspect it closer.

The Bose–Hubbard model of Eq. (34) unexpectedly has phases depending on its parameters W, U and J. Continuing from the topic of decoherence, the usual and expected result is that the system thermalizes under decoherence. We studied this thermalization phase and saw that there could exist another phase that does not thermalize. This phase is called Anderson localization or localized phase in the case where only one particle in the system was not thermalizing. From this we continued to the many-body localization. The many-body localization is a phase where every part of the system experiences slow thermalization so that the particles in the system can be seen almost in the Anderson localized phase. This phase was then said to arise in the Bose–Hubbard model if the disorder parameter reaches a certain limit.

This phase transition was what interested us in this thesis and was the focal point in all of the theoretical work we put into it. After learning all of the core features about this topic we moved onto the practicalities and constructed a simulation in which we simulated the array of transmons using a modified Bose–Hubbard model, Eq. (35). The point of this simulation was to find out the dephasing rate R_2 for the driven test transmon. This rate was used to see the phase transition in the transmons as well as the effect of the dephasing present.

The simulations were chosen to run with parameter ratio $W/J \in [1, 25]$ over three separate values of ratio U/J, which were chosen to be 2, 3.5 and 5. The results of these simulations, the dephasing rate R_2, was plotted in Fig. 11. From these results we saw that the expected thermalization phase was present in low values of W/J and the phase transition took place roughly at the same place in all of the simulation batches. We also saw that the many-body localization phase was present in the higher values of W/J, indicated by the dephasing rate R_2 which was reduced significantly.

Overall the simulations were successful as the phase transition between the thermalization and many-body localization were observed. However, the results of the fitting function were hard to interpret at the low values of W/J where the dephasing rate was so high that the averaged population difference decayed

fast. This lead to a big variance in the values of the dephasing rate, causing the results to vary.

Another critique of the simulations is that the simulation considered the transmons as three-state objects. The inclusion of higher-lying states could have lead to more accurate results. Also a smaller time step could have also improved the simulation results. Generally there were more smaller particularities that we did not account for, like choosing more points for the values of W/J.

To continue this research, one possibility would be to redo the simulations with the previous improvements and to use more accurate and faster methods of simulation like the C-programming language and its quantum computation libraries. Another research topic could be to start from the topic of pulses and their implementation to the simulations. A real-world measurement of transmons would also be one topic of interest, given expensive one.

Personally, I would continue from this thesis to the experimental side to research the pulse technology onto the transmons. Given the recent research articles we look at in the next section, the development of the technology so far interests me.

7.3 Outlook

For the last topic, we take a look at recent research articles that are related to the topics of this thesis. The research of quantum computers has advanced a lot. The topic of this thesis is part of the ongoing research to prolong the lifespan of a quantum state. The current problem we are faced with is the $1/$f-noise [16, 17] that is affecting the transmons and causing decoherence [4, 26].

Recently, new studies have experimentally measured the noise in the transmons [5, 30, 31]. These studies shed light to the $1/$f-noise in order to get rid of it. An additional computational article to accompany these studies examines the errors in the transmons [32]. With these and other research on the topic we are steadily approaching appropriate understanding of the noise in the transmons.

Another important topic that is heavily studied is the application of pulses to the transmons in order to keep the coherence. One recently published article on this topic is an experimental study of dynamical decoupling pulse scheme [33], in which Pokharel et al. demonstrates an improvement of fidelity. While there has been other research on the effects of dynamical decoupling scheme [20–23], experimental publications do not suffer from the possible errors caused by approximations.

More work on the pulses includes their optimization [34–37]. Different routes, such as pulse shape [34, 35] or distortion control [36, 37], have been considered in these articles. In order to achieve a small decoherence rate, especially in sensitive devices such as transmons, we need to optimize and fine-tune every aspect of the system. Such an optimization is difficult, but with more research it is achievable. More general optimization articles have also been published [38, 39].

Lastly, there have also been publications that focus on the same topic as us: the phase transition between the thermal phase and the many-body localization. One such work [10] examines the phase transition in more detail than us did in this thesis work measuring both experimental and computational systems. This article gives closure to one of the proposed research topics, having both experimental data of the transmons and accurate additional computational simulations.

Another article on the many-body localization topic is centered around precise measurement of the phase [11]. In this experimental article Chiaro et al. measures the many-body localization phase on a system of coupled superconducting qubits by implementing phase sensitive measurements. This allows the characterization of the many-body localization, which would otherwise require more difficult and expensive measurements techniques.

One aspect of the phase transition, the transition point or the mobility edge, has been mentioned a couple of times. A recent article characterizing this transition [12] focuses on this particular topic. In this article Gong et al. proposes a protocol and experimentally realizes it in order to detect the mobility edge. Noting a concern from the previous article, this protocol remarkably does not demand costly equipment and measurements, and is even scalable.

References

[1] T. Ladd, F. Jelezko, R. Laflamme, Y. Nakamura, C. Monroe, and J. O'Brien, "Quantum computers," *Nature*, vol. 464, no. 7285, pp. 45–53, 2010.

[2] A. Blais, S. Girvin, and W. Oliver, "Quantum information processing and quantum optics with circuit quantum electrodynamics," *Nature Physics*, vol. 16, no. 3, pp. 247–256, 2020.

[3] J. Koch, T. M. Yu, J. Gambetta, A. A. Houck, D. I. Schuster, J. Majer, A. Blais, M. H. Devoret, S. M. Girvin, and R. J. Schoelkopf, "Charge-insensitive qubit design derived from the Cooper pair box," *Phys. Rev. A*, vol. 76, p. 042319, Oct. 2007.

[4] S. M. Girvin, *Circuit QED: Superconducting Qubits Coupled to Microwave Photons, in Proceedings of the 2011 Les Houches Summer School on Quantum Machines, eds. M. H. Devoret, R. J. Schoelkopf and B. Huard*. Oxford University Press, 2014.

[5] G. Park, G. Choi, J. Choi, J. Choi, S.-G. Lee, K.-W. Lee, W. Song, and Y. Chong, "Observation of a strongly enhanced relaxation time of an in-situ tunable transmon on a silicon substrate up to the purcell limit approaching 100 μs," *Journal of the Korean Physical Society*, vol. 76, no. 11, pp. 1029–1034, 2020.

[6] R. Nandkishore and D. A. Huse, "Many-Body Localization and Thermalization in Quantum Statistical Mechanics," *Annu. Rev. of Condens. Matter Phys.*, vol. 6, no. 1, pp. 15–38, 2015.

[7] E. Altman and R. Vosk, "Universal Dynamics and Renormalization in Many-Body-Localized Systems," *Annu. Rev. of Condens. Matter Phys.*, vol. 6, no. 1, pp. 383–409, 2015.

[8] T. Orell, A. A. Michailidis, M. Serbyn, and M. Silveri, "Probing the many-body localization phase transition with superconducting circuits," *Physical Review B*, vol. 100, Oct 2019.

[9] P. W. Anderson, "Absence of diffusion in certain random lattices," *Phys. Rev.*, vol. 109, pp. 1492–1505, Mar 1958.

[10] Q. Guo, C. Cheng, Z.-H. Sun, Z. Song, H. Li, Z. Wang, W. Ren, H. Dong, D. Zheng, Y.-R. Zhang, R. Mondaini, H. Fan, and H. Wang, "Observation of energy-resolved many-body localization," *Nature Physics*, 2020.

[11] B. Chiaro, C. Neill, A. Bohrdt, M. Filippone, F. Arute, K. Arya, R. Babbush, D. Bacon, J. Bardin, R. Barends, S. Boixo, D. Buell, B. Burkett, Y. Chen, Z. Chen, R. Collins, A. Dunsworth, E. Farhi, A. Fowler, B. Foxen, C. Gidney,

M. Giustina, M. Harrigan, T. Huang, S. Isakov, E. Jeffrey, Z. Jiang, D. Kafri, K. Kechedzhi, J. Kelly, P. Klimov, A. Korotkov, F. Kostritsa, D. Landhuis, E. Lucero, J. McClean, X. Mi, A. Megrant, M. Mohseni, J. Mutus, M. McEwen, O. Naaman, M. Neeley, M. Niu, A. Petukhov, C. Quintana, N. Rubin, D. Sank, K. Satzinger, A. Vainsencher, T. White, Z. Yao, P. Yeh, A. Zalcman, V. Smelyanskiy, H. Neven, S. Gopalakrishnan, D. Abanin, M. Knap, J. Martinis, and P. Roushan, "Direct measurement of non-local interactions in the many-body localized phase," 2020. arXiv:1910.06024.

[12] M. Gong, G. D. de Moraes Neto, C. Zha, Y. Wu, H. Rong, Y. Ye, S. Li, Q. Zhu, S. Wang, Y. Zhao, F. Liang, J. Lin, Y. Xu, C.-Z. Peng, H. Deng, A. Bayat, X. Zhu, and J.-W. Pan, "Experimental characterization of quantum many-body localization transition," 2020. arXiv:2012.11521.

[13] J. Tuorila, "Kvanttimekaniikka ii." University of Oulu, 17 April 2015.

[14] M. Silveri and E. Thuneberg, "Quantum devices." Research Unit of Nano and Molecular Systems, University of Oulu, 21 October 2019.

[15] K. Jacobs, *Stochastic processes for physicists : understanding noisy systems*. Cambridge. UK ; New York: Cambridge University Press, 2010.

[16] E. Milotti, "1/f noise: a pedagogical review," 2002. arXiv:physics/0204033.

[17] J. Timmer and M. Koenig, "On generating power law noise.," *Astronomy and Astrophysics*, vol. 300, p. 707, Aug 1995.

[18] C. A. Brasil, F. F. Fanchini, and R. d. J. Napolitano, "A simple derivation of the lindblad equation," *Revista Brasileira de Ensino de Física*, vol. 35, p. 01–09, Mar 2013.

[19] M. Serbyn, M. Knap, S. Gopalakrishnan, Z. Papić, N. Yao, C. Laumann, D. Abanin, M. Lukin, and E. Demler, "Interferometric Probes of Many-Body Localization," *Phys. Rev.Lett.*, vol. 113, p. 147204, Oct. 2014.

[20] G. S. Uhrig, "Keeping a quantum bit alive by optimized π-pulse sequences," *Phys. Rev. Lett.*, vol. 98, p. 100504, Mar 2007.

[21] G. S. Uhrig, "Exact results on dynamical decoupling by π pulses in quantum information processes," *New Journal of Physics*, vol. 10, p. 083024, aug 2008.

[22] L. Cywiński, R. M. Lutchyn, C. P. Nave, and S. Das Sarma, "How to enhance dephasing time in superconducting qubits," *Phys. Rev. B*, vol. 77, p. 174509, May 2008.

[23] A. M. Souza, G. A. Álvarez, and D. Suter, "Robust dynamical decoupling," *Philos. Trans. R. Soc. London, Ser. A*, vol. 370, no. 1976, pp. 4748–4769, 2012.

[24] J. Keeler, *Understanding NMR spectroscopy*. Chichester, U.K.: John Wiley and Sons, 2nd ed ed., 2010.

[25] P. Roushan, C. Neill, J. Tangpanitanon, V. M. Bastidas, A. Megrant, R. Barends, Y. Chen, Z. Chen, B. Chiaro, A. Dunsworth, A. Fowler, B. Foxen, M. Giustina, E. Jeffrey, J. Kelly, E. Lucero, J. Mutus, M. Neeley, C. Quintana, D. Sank, A. Vainsencher, J. Wenner, T. White, H. Neven, D. G. Angelakis, and J. Martinis, "Spectroscopic signatures of localization with interacting photons in superconducting qubits," *Science*, vol. 358, pp. 1175–1179, Dec. 2017.

[26] J. Bergli, Y. M. Galperin, and B. L. Altshuler, "Decoherence in qubits due to low-frequency noise," *New Journal of Physics*, vol. 11, p. 025002, feb 2009.

[27] J. Johansson, P. Nation, and F. Nori, "QuTiP: An open-source python framework for the dynamics of open quantum systems," *Computer Physics Communications*, vol. 183, pp. 1760–1772, aug 2012.

[28] J. Johansson, P. Nation, and F. Nori, "QuTiP 2: A python framework for the dynamics of open quantum systems," *Computer Physics Communications*, vol. 184, pp. 1234–1240, apr 2013.

[29] D. A. Steck. Quantum and Atom Optics, available online at http://steck.us/teaching (revision 0.13.4, 24 September 2020).

[30] S. Schlör, J. Lisenfeld, C. Müller, A. Bilmes, A. Schneider, D. Pappas, A. Ustinov, and M. Weides, "Correlating decoherence in transmon qubits: Low frequency noise by single fluctuators," *Phys. Rev. Lett*, vol. 123, no. 19, 2019.

[31] J. Burnett, A. Bengtsson, M. Scigliuzzo, D. Niepce, M. Kudra, P. Delsing, and J. Bylander, "Decoherence benchmarking of superconducting qubits," *npj Quantum Information*, vol. 5, no. 1, 2019.

[32] D. Willsch, M. Nocon, F. Jin, H. De Raedt, and K. Michielsen, "Gate-error analysis in simulations of quantum computers with transmon qubits," *Phys. Rev. A*, vol. 96, no. 6, 2017.

[33] B. Pokharel, N. Anand, B. Fortman, and D. Lidar, "Demonstration of fidelity improvement using dynamical decoupling with superconducting qubits," *Phys. Rev. Lett*, vol. 121, no. 22, 2018.

[34] M. Werninghaus, D. Egger, F. Roy, S. Machnes, F. Wilhelm, and S. Filipp, "Leakage reduction in fast superconducting qubit gates via optimal control," *npj Quantum Information*, vol. 7, no. 1, 2021.

[35] S. Machnes, E. Assémat, D. Tannor, and F. Wilhelm, "Tunable, flexible, and efficient optimization of control pulses for practical qubits," *Phys. Rev. Lett*, vol. 120, no. 15, 2018.

[36] M. Rol, L. Ciorciaro, F. Malinowski, B. Tarasinski, R. Sagastizabal, C. Bultink, Y. Salathe, N. Haandbaek, J. Sedivy, and L. Dicarlo, "Time-domain characterization and correction of on-chip distortion of control pulses in a quantum processor," *Appl. Phys. Lett.*, vol. 116, no. 5, 2020.

[37] S. Gustavsson, O. Zwier, J. Bylander, F. Yan, F. Yoshihara, Y. Nakamura, T. Orlando, and W. Oliver, "Improving quantum gate fidelities by using a qubit to measure microwave pulse distortions," *Phys. Rev. Lett*, vol. 110, no. 4, 2013.

[38] S. Glaser, U. Boscain, T. Calarco, C. Koch, W. Köckenberger, R. Kosloff, I. Kuprov, B. Luy, S. Schirmer, T. Schulte-Herbrüggen, D. Sugny, and F. Wilhelm, "Training schrödinger's cat: Quantum optimal control: Strategic report on current status, visions and goals for research in europe," *Eur. Phys. J. D*, vol. 69, no. 12, 2015.

[39] N. Khaneja, T. Reiss, C. Kehlet, T. Schulte-Herbrüggen, and S. Glaser, "Optimal control of coupled spin dynamics: Design of nmr pulse sequences by gradient ascent algorithms," *Journal of Magnetic Resonance*, vol. 172, no. 2, pp. 296–305, 2005.